



# Data assimilation sensitivity experiments in the East Auckland Current system using 4D-Var

Rafael Santana<sup>1,2,3</sup>, Helen Macdonald<sup>2</sup>, Joanne O’Callaghan<sup>1</sup>, Brian Powell<sup>4</sup>, Sarah Wakes<sup>3</sup>, and Sutara H. Suanda<sup>5</sup>

<sup>1</sup>The University of Auckland, Department of Physics, Auckland, 1010, New Zealand

<sup>2</sup>National Institute of Water and Atmospheric Research, Wellington, 6021, New Zealand

<sup>3</sup>University of Otago, Department of Mathematics & Statistics, Dunedin, 9016, New Zealand

<sup>4</sup>Department of Oceanography, University of Hawai’i, Honolulu, HI 96822, United States

<sup>5</sup>University of North Carolina Wilmington, Wilmington, NC, 28403, United States

**Correspondence:** Rafael Santana (rafacsantana@gmail.com)

**Abstract.** This study analyses data assimilative numerical simulations in an eddy dominated western boundary current: the East Auckland Current (EAuC). The goal is to assess the impact of assimilating surface and subsurface data into a model of the EAuC. We used the Regional Ocean Modelling System (ROMS) in conjunction with the 4-dimensional variational (4D-Var) data assimilation scheme to incorporate sea surface height (SSH) and temperature (SST), and subsurface temperature, salinity, and velocities from three moorings located at the upper, mid and lower continental slope using a 7-day assimilation window. Assimilation of surface fields (SSH and SST) reduced SSH root mean square deviation (rmsd) in relation to the non-assimilative (NoDA) run. The inclusion of velocity subsurface data reduced SSH rmsd up- and downstream the moorings. By improving the representation of the mesoscale eddy field, data assimilation increased complex correlation between modelled and observed velocity in all experiments. However, the inclusion of temperature and salinity slightly decreased the velocity complex correlation. The assimilative experiments had smaller SST rmsd in comparison to the NoDA run. The lack of subsurface temperature for assimilation led to larger errors ( $>1^{\circ}\text{C}$ ) around 100 m in relation to the NoDA run. Comparisons to independent Argo data showed similar results. Withholding subsurface temperature forces near-surface average negative temperature increments that are corrected by increased net heat flux at the surface which does not affect waters at 100 m depth. Assimilation of mooring temperature generates increments to the initial conditions that reduces 100 m water temperature rmsd. Larger positive wind stress curl was generated in experiments that assimilated subsurface temperature data. Positive wind stress curl generates convergence and downwelling which is another way of correcting the upper thermocline cold bias. The larger positive wind stress curl might also be responsible for decreased velocity correlation in the experiments that assimilated temperature and salinity. The few moored CTDs (8) had little impact in correcting salinity, however, using doubled decorrelation length scales of tracers and a 2-day assimilation window improved model salinity in comparison to independent Argo data. In addition, the results were similar to the global reanalysis HYCOM-NCODA which assimilates Argo profiles and was used as boundary condition. HYCOM-NCODA had near zero velocity complex correlation on the mid-slope, whereas all reanalyses showed improved results which highlights the benefit of downscaling to a regional model of the EAuC.



## 1 Introduction

The East Auckland Current (EAuC) is a western boundary current (WBC) that originates as the reattachment of the subtropical water flow to a continental margin on the New Zealand Northeastern Continental Slope (NZNES) (Stanton et al. (1997), Fig. 1). The EAuC mean transport was estimated to be 9 Sverdrups (Sv) (Roemmich and Sutton, 1998) with variability at periods longer than 100 days (Stanton and Sutton, 2003). Studies of the EAuC impact on the continental shelf found shallow (60 m) intrusions of subtropical water, possibly driven by EAuC bottom Ekman transport (Zeldis et al., 2004; Santana et al., 2021). Long-term variability (> 100 days) in the EAuC was suggested to be driven by the arrival of baroclinic Rossby waves (Laing et al., 1998; Chiswell, 2001). Santana et al. (2021) observed locally formed mesoscale eddies and their arrival from the east using a one-year time series of in situ and remotely-sensed data. The EAuC is less coherent compared to other WBC, where its ratio between the eddy and mean kinetic energies is larger than the East Australian Current's (EAC) ratio (Oke et al., 2019). Mesoscale eddies are generated by barotropic and baroclinic instabilities, which are unpredictable (Marchesiello et al., 2003; Feng et al., 2005), and accurate simulation of the EAuC variability needs to incorporate observations to realistically represent eddies and other features that vary on short timeframes (Oke et al., 2005, 2013, 2015; Santana et al., 2020).

Data assimilation (DA) combines observations and numerical models to obtain ocean fields with reduced uncertainty, called the analysis, that better represents the ocean state (e.g. location of mesoscale eddies). The ocean analysis can be achieved via calculus of variations through the minimisation, in a least-squares sense, of the difference between model results and observations (Weaver et al., 2003; Di Lorenzo et al., 2007; Moore et al., 2011b). The 4-dimensional variational data assimilation (4D-Var) method reduces model errors over a finite time interval using all observations available while preserving dynamical consistency. 4D-Var has notable applications in oceanography, such as: Weaver et al. (2003); Powell et al. (2008); Mazloff et al. (2010); Matthews et al. (2012); Zavala-Garay et al. (2012); de Souza et al. (2015); Osafune et al. (2015); Kerry et al. (2016); Powell (2017); Phillipson and Toumi (2017); Pasmans et al. (2019); Janeković et al. (2020); Siripatana et al. (2020); Levin et al. (2020); López et al. (2020); de Paula et al. (2021); Moore et al. (2021)). Some of those are realistic 4D-Var applications using the Regional Ocean Modelling system (ROMS), from which different values of time-window length, observational errors, and decorrelation length scales were used for the tests presented in the current study.

Observing system experiments (OSEs) aim to assess the importance of distinct sets of observations on the quality of different analyses (Oke et al., 2015). By withholding observational subsets, one can estimate the importance of those data in the ocean reanalysis. For instance, Zavala-Garay et al. (2012) used ROMS 4D-Var to show that assimilation of sea surface temperature (SST) and height (SSH) data only increased temperature error between 350 and 750 m in comparison to a non-assimilative run. The authors found that assimilation of XBT or synthetic CTD data were needed to correct this. Pasmans et al. (2019) stated that assimilation of temperature and salinity from ocean gliders should be accompanied by surface measurements to prevent the generation of unrealistic instabilities. Siripatana et al. (2020) compared two reanalysis: (i) assimilated traditional observations only (satellite SSH and SST, and temperature and salinity from Argo floats) and (ii) assimilated traditional observations and data from moorings, gliders and high-frequency radar; and found improved subsurface results in the latter experiment.



The EAuC system lacks traditional subsurface data, where Argo profiles are rare and the region can experience months without any water column measurement. Between May 2015 and May 2016, the EAuC region was sampled along Topex/Poseidon 147 line, when five mooring lines (named M1 to M5) were deployed from coastal waters to the continental rise which sampled velocity, temperature and salinity (Fig. 1) and analysed in Santana et al. (2021). Sampling efforts like those are costly, and deciding important variables and locations of interest for ocean sampling is key in the region, specially in this eddy dominated WBC. Moreover, the EAuC also showed strong velocity shear on the continental mid-slope (Santana et al., 2021), which might indicate the need for subsurface data for accurate velocity simulation.

The goal of this study is to evaluate the impact of subsurface data assimilation into a model of EAuC system. We conducted a set of OSEs where the most complete simulation assimilated surface fields (SSH and SST), and mooring velocity, temperature and salinity (ASFUVTS) (Fig. 1). The other experiments suppressed observation types in the assimilation algorithm. They withheld velocities (NoUV); subsurface temperature and salinity (NoTS); and all mooring data (NoUVTS). As control, we examined a non-assimilative freely evolving simulation (NoDA). Argo data was left out of all experiments for independent model-data comparison.

## 2 Methods

### 2.1 Numerical model

We use the Regional Ocean Modeling System (ROMS), a primitive-equation, hydrostatic, and free-surface ocean model that solves the Reynolds-averaged form of the Navier–Stokes equations. ROMS is a fully nonlinear, finite-difference model that uses terrain-following (sigma) vertical coordinates and horizontal orthogonal or curvilinear Arakawa C grid (Shchepetkin and McWilliams, 2003, 2005; Haidvogel et al., 2008). The model domain (290 x 150) is rotated 52.14° clockwise to better resolve the NZNES and spans 332 km offshore at the widest point (near North Cape) (Fig. 1). The domain has horizontal resolution of approximately 2 km, which roughly captures coastline variability and still resolves the continental shelf and slope without large computational cost. The model has 30 vertical sigma layers and model bathymetry was interpolated from the 250 m resolution bathymetric data set built by the National Institute of Water and Atmospheric Research (NIWA - <https://niwa.co.nz/our-science/oceans/bathymetry>). We use a vertical discretisation scheme that increases the resolution near the surface and bottom by applying stretching function type 4 and transformation equation option 2 (Shchepetkin and McWilliams, 2005, 2009). The vertical resolution is higher at the upper 200 m (from 4 to 30 layers). On the slope (depth < 1000 m), the vertical resolution is higher than 66 m and in the open ocean the thickest level is 233 m (3838.6 m depth). Baroclinic modes are resolved using a time step of 180 s, while the barotropic time step is 6 s.

Model surface forcing is from the Japanese atmospheric 55-year reanalysis for driving ocean models (JRA55-do, Tsujino et al. (2018)). A previous study demonstrated that JRA55-do had the highest correlation with observed winds in comparison to other atmospheric forcing datasets in the Southwest Pacific (Taboada et al., 2019). Atmospheric forcing fields of wind speed, net shortwave radiation, downward longwave radiation, relative humidity, temperature, rain, and pressure are specified every 3 h and used to compute the surface fluxes of stress, heat and freshwater using the bulk flux parameterisation of Fairall

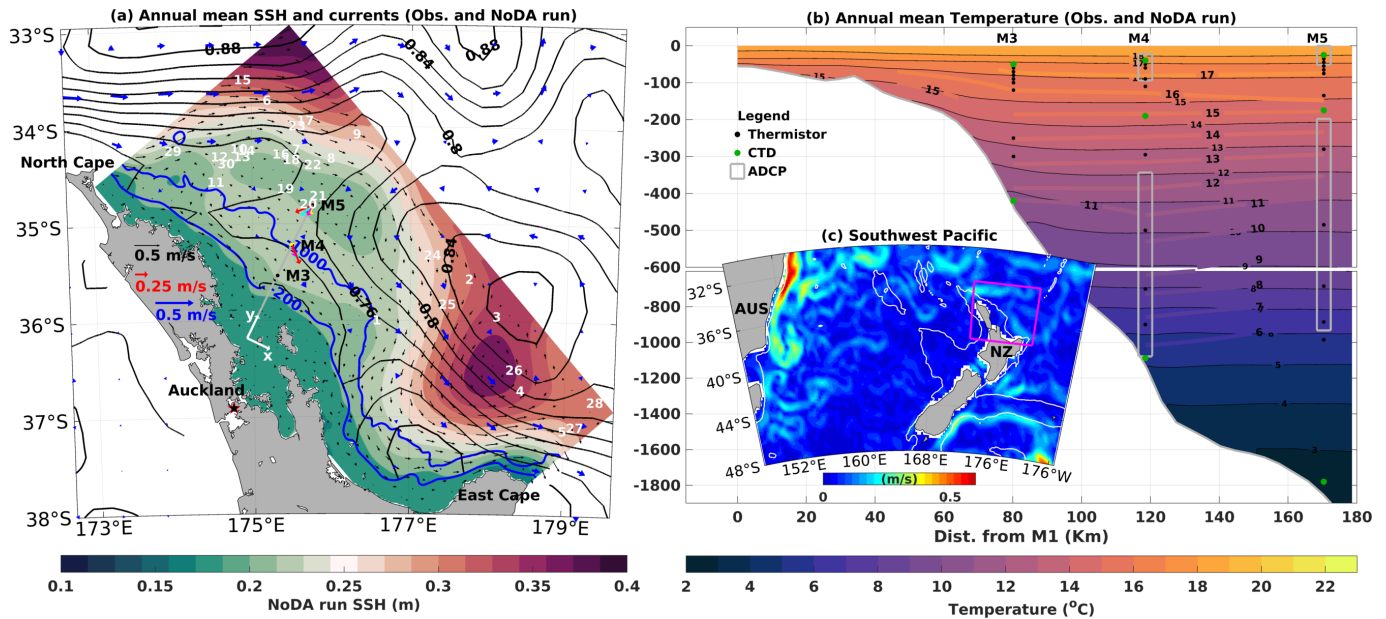


**Figure 1.** (a) Study area showing the one-year average SSH from AVISO (black contours) and NoDA run (green-red shade), geostrophic velocities from AVISO (blue arrows) and NoDA run (black arrows). The coloured arrows represent the vertically averaged (bin = 280 m) *in situ* velocities centered at 140 m (red), 420 m (cyan), 700 m (blue), and 980 m (yellow). The white arrows represent the orientation axes used. The stations M3 to M5 are indicated along the grey line. Integer numbers represent Argo locations for independent data comparison. (b) Temporal averages of temperature from in situ measurements (coloured contours) and the NoDA run (coloured shade). The grey rectangles show regions sampled by ADCPs at M4 and M5 and used in data assimilation. The vertical positions of thermistors and CTDs are indicated as black and green dots, respectively. (c) Location of the study area (magenta contour) relative to other currents in the Southwestern Pacific Ocean. The colors represent the one-year average of geostrophic current speed. The 200- and 1000-meter isobaths are shown as blue and white contours in (a) and (c).

et al. (2003). The model uses initial and boundary conditions of SSH, temperature, salinity, and velocities from HYCOM-NCODA (Chassignet et al., 2009) versions 91.1 and 91.2 which cover period of simulations generated here. de Souza et al. (2021) analysed the performance of four global reanalysis that assimilate SSH, SST and Argo data on the New Zealand waters. The authors found that HYCOM-NCODA (8 km resolution) had higher SSH and SST variability than low-resolution (25 km) satellite surface observations and other reanalyses with similar grid-spacing. HYCOM-NCODA had velocity standard deviation similar to that observed at M4 and M5, even though GLORYS (8 km global ocean reanalysis, (Lellouche et al., 2018)) better represented temperature and salinity profiles in the region. Annual average discharge from several rivers are included as lateral forcing in the model. The boundary forcing is applied daily using Chapman (1985) condition for free surface, Shchepetkin condition (Mason et al., 2010) for barotropic velocities and mixed radiation-nudging (Marchesiello et al., 2001) for baroclinic velocities, temperature and salinity. A 5-day nudging coefficient is applied towards the lateral boundaries. The model aims to simulate continental shelf, slope and rise regions, including the offshore extent of the EAUC and its eddy variability. This



100 and the upcoming studies using the simulations analysed here focus on intra-annual variability and tides are not included as forcing.

## 2.2 Observations

Remotely-sensed observations of SSH and SST were used in all assimilative runs of the current study. Optimally interpolated gridded maps of daily SSH with  $1/4^\circ$  of horizontal resolution created by AVISO (Ducet et al., 2000) were assimilated into the model. Daily SSH offsets (annual mean of  $\sim 51$  cm) were calculated prior to every assimilation cycle as the difference between the spatial average of observations and model daily averages for each assimilative experiment (one-year averages are shown in Fig. 1a as examples of this offset). This offset was removed from AVISO observations before assimilation to ensure the comparisons were made on the same reference surface. Daily maps of SST ( $1/4^\circ$ ) from AVHRR Pathfinder (Casey et al., 2010) were used for assimilation into the model at a depth of 2 m. SSH and SST data were assimilated daily at 12:00 pm UTC in regions deeper than 200 m. Data points that are within 20 grid points of the boundaries were removed and a total of 123 data points of SSH (or SST) were assimilated per day, with roughly an SSH/SST measurement every  $12^{th}$  grid point. We used an assimilation window of seven days (see details in section 2.3) which gives a total of 861 SSH/SST data points per assimilation cycle (Fig. 2).

A cross shelf-slope mooring transect collected data from the 6th of May 2015 and the 21st of May 2016 (Fig 1a,b). In situ observations of temperature, salinity, u and v components of velocity from moorings M3, M4, and M5 were assimilated into the model (Fig 1b). MicroCAT CTDs were located near the surface and bottom at the three stations and two extras CTDs were located around 200 m at M4 and M5 (green dots in Fig 1b). 26 temperature sensors were evenly distributed between the three stations, with higher density of instruments in the upper 200 m water column (black dots in Fig 1b). Two long range (LR) and two short range (SR) ADCPs were located at M4 and M5 (grey rectangles in Fig 1b). The water column was binned every 15 m (LR) or 4 m (SR) by the upward looking ADCPs. Velocity (temperature and salinity) measurements were taken during a period of 2 min. (1 min.) every 10 min or less. The dataset is freely available and can be found in O'Callaghan et al. (2015). All in situ observations were low-pass filtered at a period of 30h to remove tidal signals and their interaction with other processes, as in Kerry et al. (2016). The observations were averaged at time bins of 6 h, centred at 3, 9, 15 and 21 UTC. Mooring velocity observations (magenta line in Fig. 2) were available in the first cycle and were followed by temperature and salinity (cyan and green lines in Fig. 2). Velocity had the largest amount of mooring observations but stratification information (SST, mooring temperature and salinity) was larger when combined (blue line in Fig. 2).

Non-assimilated data from 30 Argo profiles (Roemmich et al., 2019) sampled the region encompassed by the model domain (integer numbers in Fig. 1a) during the simulation period and were used for model-data independent comparison. More details on model evaluation are described in section 2.4.

## 130 2.3 Data assimilation

Data assimilation is applied in a series of time windows using strong constraint 4D-Var, i.e. neglecting model errors (Di Lorenzo et al., 2007; Moore et al., 2011b). Tests using 2, 3, 4, and 7 days as assimilation window were conducted and the OSEs with a

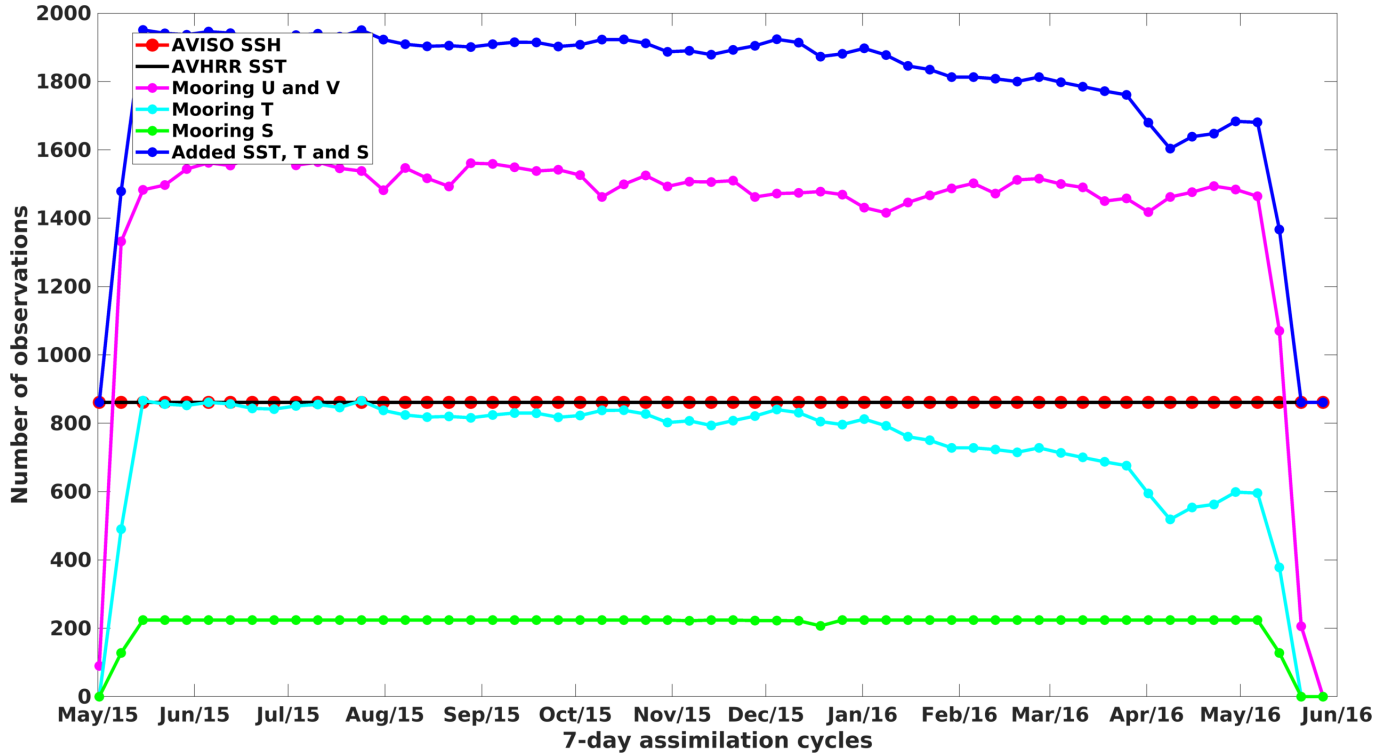


**Figure 2.** Number of observations (after quality control and assurance, filtering and averaging) used in each 7-day assimilation cycle. Observations types are shown by colour: AVISO SSH (red), AVHRR SST (black), mooring u and v components of velocity (magenta), mooring temperature (cyan), mooring salinity (green), combined SST, mooring temperature and salinity (blue). Mooring data was used from stations M3, M4 and M5.

7-day window had the most realistic results in comparison to observations. Results from a 2-day window reanalysis were also analysed in the current study. In this work, 4D-Var is used to adjust the control variables for initial, boundary, and atmospheric conditions. The ocean analysis is obtained via minimisation of model-to-data discrepancy or cost function ( $J$ ) given by:

$$J(\delta\mathbf{z}) = \frac{1}{2}\delta\mathbf{z}^T\mathbf{D}^{-1}\delta\mathbf{z} + \frac{1}{2}(\mathbf{G}\delta\mathbf{z} - \mathbf{d})^T\mathbf{R}^{-1}(\mathbf{G}\delta\mathbf{z} - \mathbf{d}) \quad (1)$$

where  $\delta\mathbf{z}$  is the state vector constituted of increments (corrections) to the initial  $\delta\mathbf{x}(t_0)$ , lateral  $\delta\mathbf{b}(t)$ , and surface  $\delta\mathbf{f}(t)$  conditions.  $\mathbf{D}$  and  $\mathbf{R}$  are the background and observation error covariance matrixes, respectively. Superscripts T and -1 represent the transpose and inverse operations, respectively.

$\mathbf{G} \equiv \mathbf{H}\mathbf{M}_f$ , where  $\mathbf{H}$ , is the linearised version of the observation function  $\mathcal{H}$  that maps the model-state to the observation time and locations. The operator  $\mathbf{M}_f$  denotes the tangent linear operator of the model integration about the forecast (denoted by the subscript f) over the assimilation window. For the transpose,  $\mathbf{G}^T \equiv \mathbf{M}_f^T\mathbf{H}^T$ ,  $\mathbf{H}^T$  maps from observation to model-space and the  $\mathbf{M}^T$  operation integrates backward in time over the assimilation window.





$\mathbf{G}\delta\mathbf{z} - \mathbf{d}$  represents the mismatch between the tangent linear model fields mapped to the observations ( $\mathbf{G}\delta\mathbf{z}$ ) and the obser-  
145 vations  $\mathbf{d}$  which is called the innovation vector and is defined as the difference between observations and model background  
interpolated to observation location. SSH observations had a daily bias (or offset) between data and model reduced from the  
observations before the innovation values were computed.

The combination of control variables  $\delta\mathbf{z}_a$  that minimizes  $\mathbf{J}$  is yielded iteratively in the subspace spanned by the linear  
combinations of the observed model variables. The method chosen in the present work is the physical-space statistical analysis  
150 system (4D-PSAS) (Moore et al., 2011b), which defines  $\delta\mathbf{z}_a$  as:

$$\delta\mathbf{z}_a = \mathbf{D}\mathbf{G}^T(\mathbf{G}\mathbf{D}\mathbf{G}^T + \mathbf{R})^{-1}\mathbf{d} \quad (2)$$

$\delta\mathbf{z}_a$  can be equivalently written as  $\delta\mathbf{z}_a = \mathbf{D}\mathbf{G}^T\mathbf{w}^a$  where  $\mathbf{w}^a$  is the sub-space of the model state vector spanned by the observa-  
tions (i.e. the dual space) and satisfies:

$$(\mathbf{G}\mathbf{D}\mathbf{G}^T + \mathbf{R})\mathbf{w}^a = \mathbf{d} \quad (3)$$

155 The dual form has the advantage that the dimension of  $\mathbf{w}^a$  is equal to the number of observations which is, in our case, several  
orders of magnitude smaller than the dimension of the full state vector. Thus, solving (3) may be less demanding than solving  
(2) (Moore et al., 2011b).

In practice, we find an acceptable reduction of the model-to-data discrepancy after 20 iterations (inner loops), when atmo-  
spheric and lateral forcings are adjusted every 12 h along with initial conditions at the beginning of the assimilation cycle. For  
160 further details of the method and its application, readers are referred to Moore et al. (2011b, a).

The background error covariance matrix  $\mathbf{D}$  cannot be completely calculated or stored, it is rather estimated via factorisation  
(Weaver and Courtier, 2001).  $\mathbf{D}$  takes into consideration the background error standard deviations, spatial decorrelation scales,  
and normalisation factors (Moore et al., 2011a). Background error standard deviations were calculated from the average of  
4-day variances computed from 2 years of the NoDA run. Horizontal decorrelation length scales for SSH, velocities, active  
165 tracers (temperature and salinity) were 100, 50 and 100 kilometres. Vertical decorrelation length scales for velocities and active  
tracers were 50 and 100 metres. The normalisation factors were estimated via randomisation (Fisher and Courtier, 1995) using  
7500 iterations. The described background error configuration is valid for the 7-day reanalyses which differs in three aspects  
from the 2-day reanalysis – see section 2.4 for details.

The observational error covariance matrix  $\mathbf{R}$  is assumed to be diagonal. The standard deviation used was the largest value  
170 between an assigned standard deviation and the observation error obtained from the AVISO and AVHRR products, with the  
assigned value being the highest most of the time. This strategy was applied to satellite observations, whereas in situ data used  
a given standard deviation only. According to values used in the literature (e.g. Moore et al. (2011a); Kerry et al. (2016)),  
different standard deviations were tested and the values that gave the best results were: 0.04 m for SSH; 0.3 °C for satellite  
SST; 0.8 °C for subsurface temperature; 0.16 g/kg for subsurface salinity; and 0.15 m/s for u and v components of velocities.



175 Large standard deviation was attributed to in situ temperature due to strong internal tides in the region and blow down events that often happened at the three moorings. Depth of the thermistors was obtained assuming an inverted pendulum relationship between CTDs located near the surface and bottom (Stanton and Morris, 2004) but a level of uncertainty remains in the depth of measurements.

## 2.4 Experiment design and evaluation

180 Five data assimilative experiments and one free-running simulation (no data assimilation; NoDA) were conducted. The first data assimilative experiment incorporated SSH, SST, u and v components of velocity and temperature and mooring temperature and salinity data (ASFUVTS). The other data assimilative experiments were similar but withheld: subsurface temperature and salinity (NoTS); mooring velocities (NoUV); and all mooring data (NoUVTS). Another experiment assimilating surface and all mooring data was also conducted using a 2-day assimilation window (ASFUVTS-2days) which was designed to better  
185 match the observations. This experiment (ASFUVTS-2days) differed from the other simulations in three aspects. It used 7-day variances to compute background error standard deviations and 200 kilometres (metres) as horizontal (vertical) decorrelation length scales of active tracers (temperature and salinity). The last difference is the assimilation window length which is two days. These modifications made ASFUVTS-2days less comparable to the rest of the OSE but they were needed in order to achieve the best match between assimilated and independent observations – for results, see sections 3.2 and 3.3.

190 The numerical simulations started on the 1st of May 2015 using an interpolated initial condition from HYCOM-NCODA and they ran until the 31st of May 2016. The simulations started assimilating SSH and SST observations on the 1st of May, and mooring data between the 8th of May 2015 and the 21st of May 2016. The simulations assimilated SSH and SST until the 31st of May 2016 and 57 (200) assimilation cycles were performed in the 7-day (2-day) reanalyses. The NoDA run was integrated until 31st December 2016. Model results were interpolated to the observations spatial resolution for evaluation.

195 The NoDA run and reanalyses were objectively validated using root mean square deviation (rmsd) given by:

$$rmsd = \sqrt{\frac{1}{n} \sum_{i=1}^n (x_i - y_i)^2}; \quad (4)$$

and linear correlation (r):

$$r = \frac{\sum_{i=1}^n (x_i - \bar{x})(y_i - \bar{y})}{\sqrt{\sum_{i=1}^n (x_i - \bar{x})^2} \sqrt{\sum_{i=1}^n (y_i - \bar{y})^2}}; \quad (5)$$

200 between observed ( $x$ ) and modelled ( $y$ ) results, where  $i=1,2,\dots,n$  are the observation times or locations and the averages  $\bar{\phantom{x}}$  were applied in time or space. The daily offset between observed and model SSH was removed before performing the SSH rmsd calculation. SSH and SST rmsd were computed using daily averaged model results (analysis) interpolated to observations locations inside the domain. Complex correlation (Kundu, 1976) was calculated between simulated and observed velocity vectors. Statistics computed between model and in situ observations used daily averaged data processed and studied in Santana et al. (2021). 30 Argo profiles were available inside the model domain (integer numbers in Fig. 1a) during the reanalyses period





205 and these were used to provide independent temperature and salinity data for model-data comparison. Argo data and model results were linearly interpolated from 0 to 2000 m depth using bins of 10 m. HYCOM-NCODA analyses which assimilated SSH, SST and Argo profiles (Chassignet et al., 2009) were also used in the comparison against subsurface mooring and Argo data.

### 3 Results

#### 210 3.1 DA impact on surface fields

A skillful state estimate should have rmsd to observations smaller than the typically observed standard deviation (std). The most complete ocean analysis (ASFUVTS) had smaller SSH rmsd in comparison to the observed SSH std for most of the domain (Fig. 3a,b). The NoUVTS run had similar average SSH rmsd (0.06 m) to the ASFUVTS run. However ASFUVTS had reduced SSH rmsd upstream and downstream of the moorings (Fig. 3b,c). Experiments that assimilated in situ velocities  
215 (NoTS, ASFUVTS-2days) also had positive impact on SSH representation up- and downstream the moorings (not shown). NoDA had larger SSH rmsd (0.08-0.14 m) in comparison to observed std (0.07-0.11 m) in regions deeper than 1000 m (Fig. 3a,d), where more than 4 mesoscale eddies with life span larger than a month were observed (Santana et al., 2021).

The NoDA run had average SST rmsd (0.72 °C) smaller than the average observed SST std (2.39 °C) (Fig. 3e,h). This skill was achieved by the NoDA run's ability to reproduce the seasonal cycle (amplitude of 6 °C), however this simulation had a  
220 daily variability different to the observed. The experiment NoDA had the largest SST rmsd (>1.4 °C) near the model NW boundary, which was also seen in the assimilative runs (Fig. 3f,g,h). Assimilation of surface and subsurface fields (ASFUVTS run) reduced the maximum (~ 1.0 °C) and average (0.45 °C) SST rmsd values in comparison to the NoDA run (Fig. 3f,h). Withholding subsurface temperature data (NoUVTS runs) had small impacts in the maximum (decrease of ~ 0.2 °C) and mean (increase of 0.01 °C) SST rmsd (Fig. 3f,g), as well as for NoUV and NoTS runs (not shown).

225 The NoDA run had larger spatially averaged SSH rmsd (mean = 8 cm) in comparison to the observed spatially averaged SSH std (mean = 7 cm) for most of the year-long period of simulation (Fig. 4a). This shows the lack of skill in simulating the timing and location of the mesoscale eddies in the NoDA run. ASFUVTS and NoUVTS runs had lower temporally averaged spatial SSH rmsd (Fig. 4a) and higher temporally averaged spatial SSH correlation (Fig. 4b) in comparison to the NoDA run. ASFUVTS had even higher spatial SSH correlation which means that including subsurface data for assimilation improved  
230 the representation of mesoscale eddies and the EAuC studied in Santana et al. (2021). The SSH represents the integral of subsurface density fields which is good proxy for representation of the whole ocean state and the SSH was better represented when velocity, temperature and salinity observations were assimilated.

The NoDA run had spatial SST rmsd similar or smaller to the observed spatial SST std in the first two thirds of the simulation period, however it showed larger errors from Feb. 2016 onwards (Fig. 4c). ASFUVTS run had smaller SST rmsd time mean  
235 (0.47°C) in relation to the NoDA run (mean = 0.68°C). Withholding subsurface data (NoUVTS) had little impact in the SST rmsd (mean = 0.46°C). The NoDA run had small absolute SST difference to observations (<1.0°C) during the first two thirds of the timeseries but a larger cold bias (<-1°C) was developed in Apr. 2016 (Fig. 4d). Assimilation of surface fields

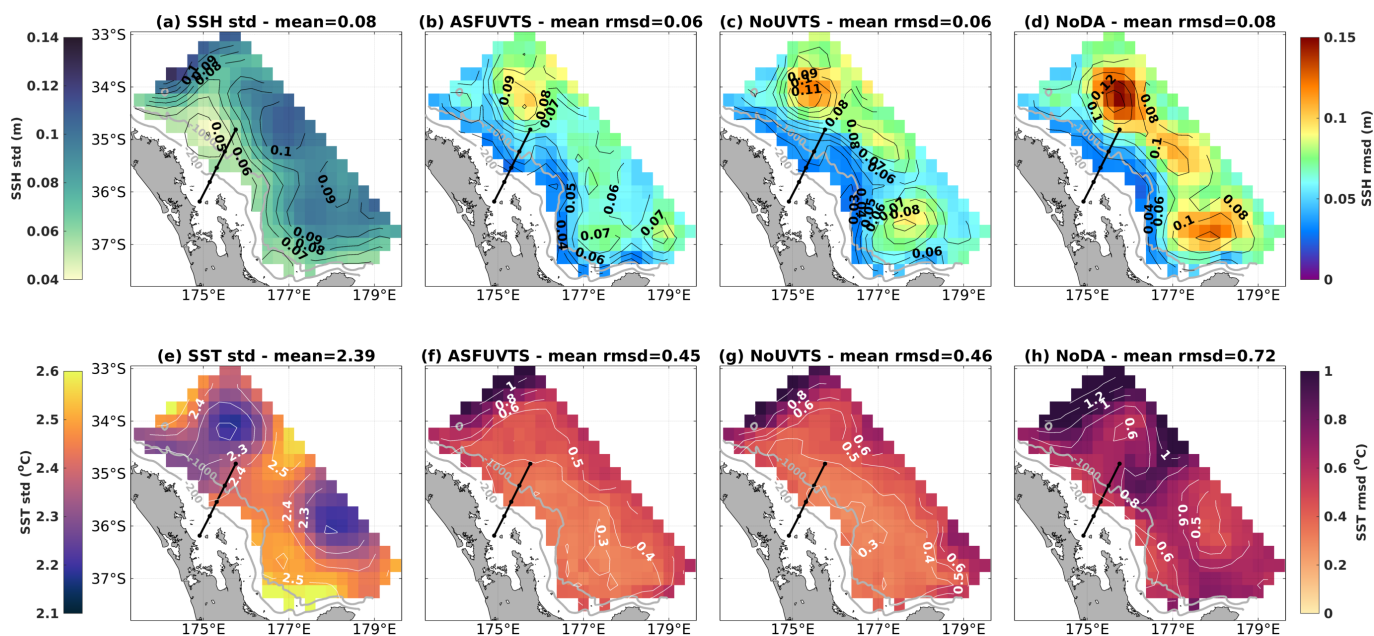


**Figure 3.** Maps of SSH (top row) and SST (bottom row) statistics. Observed AVISO SSH std (a) and AVHRR SST std (e), modelled ASFUVTS run SSH (b) and SST rmsd (f), NoUVTS SSH (c) and SST rmsd (g), NoDA SSH (d) and SST rmsd (h).

only (NoUVTS) had absolute SST bias below  $0.5^{\circ}\text{C}$  throughout the year-long period of simulation. Inclusion of subsurface data (ASFUVTS) did not have a well-marked impact on model SST bias, most of the surface field correction was done by  
 240 assimilation of SSH and SST more specifically.

Assimilation of subsurface and surface data (ASFUVTS) had little impact on the representation of SST in comparison to the experiment that withheld subsurface observations (NoUVTS). However, a positive impact was seen on the spatial SSH rmsd with respect to AVISO. Assimilation of in situ velocities reduced the SSH rmsd up- and downstream of the moorings. Main differences between experiments appeared in the subsurface fields comparisons which are shown in the next section.

### 245 3.2 DA impact on subsurface fields

The NoDA run had very little velocity complex correlation ( $< 0.1$ ) with observations at M4 and M5 (Fig. 5a,b). DA improved complex correlation between modelled and observed velocity vectors in all experiments at the two stations. These results can be related to assimilation of SSH which corrects the geostrophic circulation that is responsible for the long-term ( $> 30$  days) upper half water column current variability in the region (Santana et al., 2021). The most complete assimilative run  
 250 (ASFUVTS) had better results in comparison to NoDA but not against other assimilative runs. Withholding temperature and salinity (NoTS and NoUVTS) improved upon ASFUVTS, and NoTS had the best overall results. ASFUVTS-2days, on the other hand, had the best overall results. HYCOM-NCODA poorly represented velocity at M4 probably due to less accurate representation of the slope bathymetry (de Souza et al., 2021). At M5, however, HYCOM-NCODA showed velocity complex

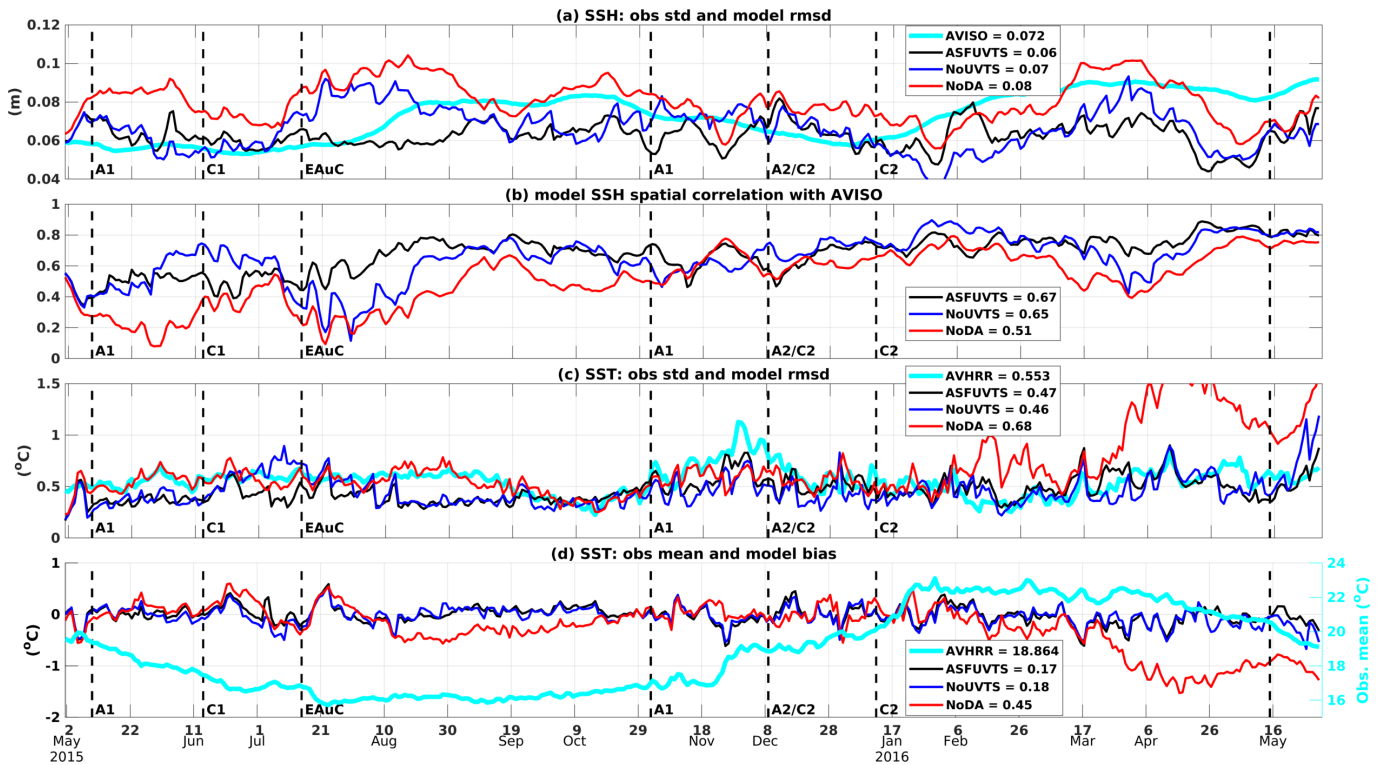


**Figure 4.** Timeseries of SSH spatial std/rmsd (a), SSH spatial correlation (b), SST spatial std/rmsd (c), and SST spatial mean or bias from AVISO/AVHRR (light blue), NoDA run (red), NoUVTS run (blue), and ASFUVTS run (black). Mean std, rmsd and correlation coefficients, and std SST bias are shown in the legend. The acronyms A1, C1, EAuC, A1, A2/C2, and C2 represent the presence of mesoscale structures at M5 studied in Santana et al. (2021).

correlation coefficient similar to the 7-day assimilative runs. Velocity at M5 was more dominated by the mesoscale field and less controlled by topographic constraints compared to M4 (Santana et al., 2021), which makes velocity easier to simulate even in lower horizontal resolution models.

The assimilative experiments had smaller temperature rmsd at the surface in comparison to the NoDA run at M4 and M5 (coloured markers at the surface in Fig. 5c,d). However, the lack of subsurface temperature for assimilation (NoTS and NoUVTS) led to larger errors ( $>1^{\circ}\text{C}$ ) in the upper 200 m at M4 and M5, and below 500 m at M5 (pink and dark blue lines in Fig. 5c,d). Assimilation of subsurface temperature (ASFUVTS and NoUV) had reduced temperature rmsd in comparison to the NoDA run from surface down to 500 m at M4 and M5 (black and light blue lines in Fig. 5c,d). ASFUVTS-2days run had improved temperature rmsd down to 1000 m at M5. HYCOM-NCODA showed improved temperature results compared to the NoDA run (dashed and solid red lines in Fig. 5c,d). This is due to the assimilation of temperature and salinity from Argo floats since the reanalysis did not assimilate data from M4 or M5.

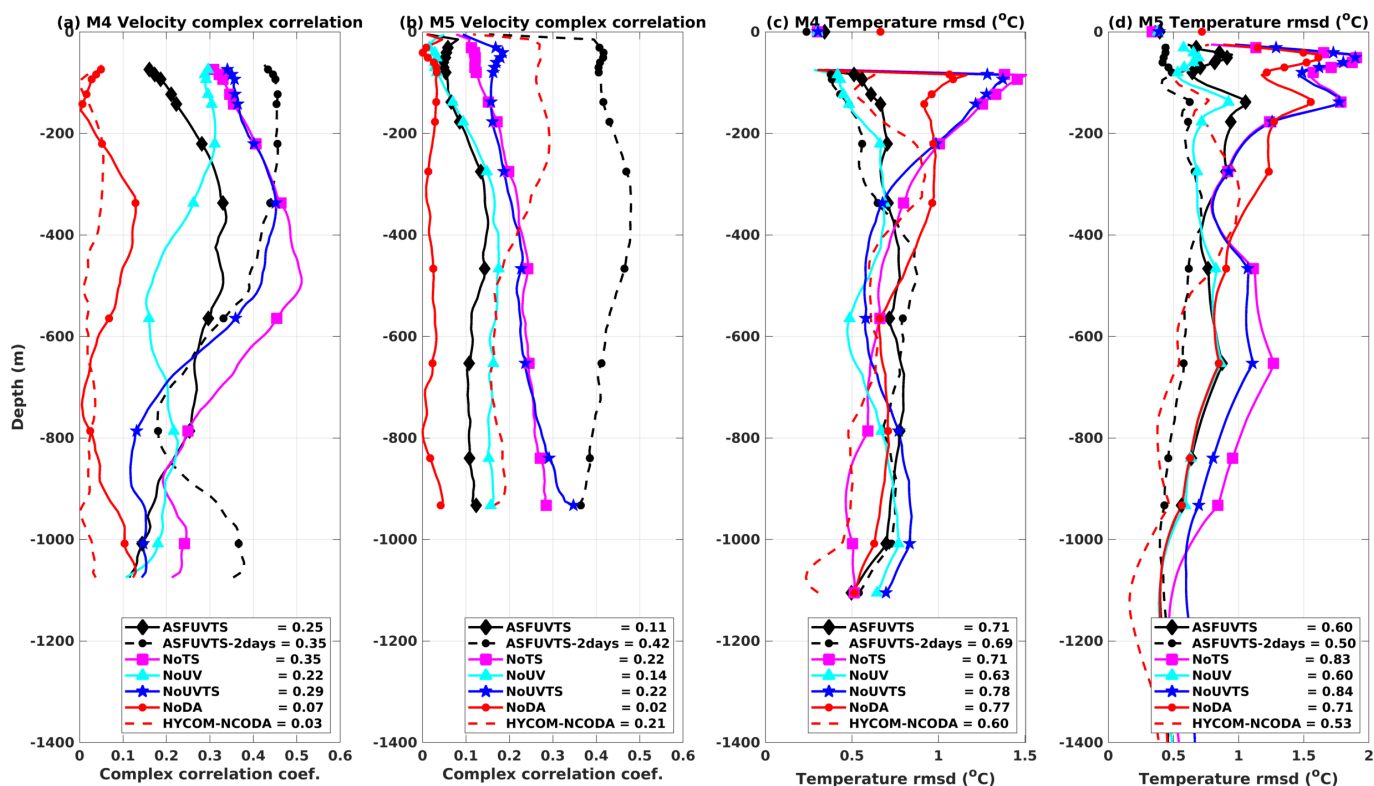


**Figure 5.** Profiles of complex correlation coefficient between observed and modelled velocity vector at (a) M4 and (b) M5. Profiles of temperature root mean square deviation between observed and modelled temperature at (c) M4 and (d) M5. Black diamonds (ASFUVTS), black dots (ASFUVTS-2days), magenta squares (NoTS), cyan triangles (NoUV), blue stars (NoUVTS) and red dots (NoDA) represent the median depth of thermistors and CTDs at each station, except at the surface where comparisons are against AVHRR SST. HYCOM-NCODA results are shown as dashed red lines. The depth averaged values of complex correlation and temperature rmsd are shown in the legend.

265 Temperature differences between model and observations at M4 showed small cold bias and relative warming at the beginning of the timeseries for all experiments (Fig. 6). The small bias can be attributed to the initial condition on 1st of May 2015 obtained from HYCOM-NCODA analysis, however, differences started to appear in Sep. 2015. ASFUVTS and NoUV runs are colder than observed between Sep. and Nov. 2015 and Mar. and May 2016 ( $<1^{\circ}\text{C}$  - second lightest blue shade in Fig. 6b,c). NoTS and NoUVTS runs are cooler in the upper 200 m water column from Sep. 2015 onwards (Fig. 6d,e). Withholding  
 270 subsurface temperature for assimilation (NoTS and NoUVTS) led to the continuous cooling of waters in the top 200 m until the end of simulation. The NoDA run had a small temperature difference when compared to observations in Sep. 2015 but these increased in Oct. 2015 (Fig. 6f). The longest persistent cold bias started in mid-Mar 2016, which might be associated with the SST cold bias during the same period (Fig. 4d). Cooling of the upper water column in the NoTS and NoUVTS runs also occurred in the NoDA run. This effect might be intrinsic to the model configuration, and data assimilation of velocities  
 275 and/or surface fields only enhanced this bias.

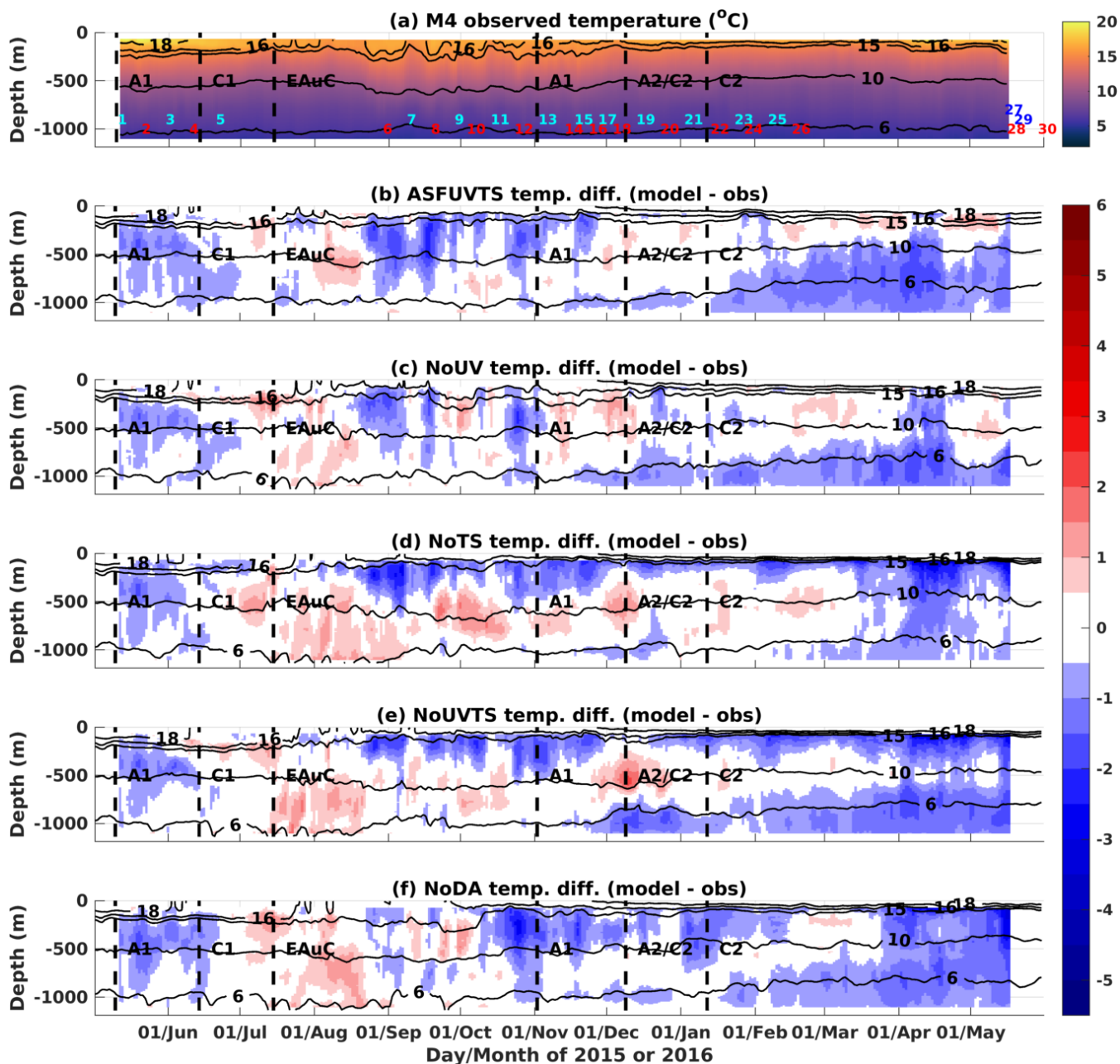


**Figure 6.** (a) M4 observed daily average temperature and difference between modelled and observed temperature for experiments (b) ASFUVTS, (c) NoUV, (d) NoTS, (e) NoUVTS and (f) NoDA. The red, blue and cyan numbers in (a) show the dates where Argo profilers sampled the NZNES. The location of the Argo floats are shown in Fig. 1a and 8e.

At M5, a mid water column warm bias ( $>1^{\circ}\text{C}$ ) was simulated in the first half of the year-long period in all experiments (second lightest red shade Fig. 7). This also happened on HYCOM-NCODA between Jun and Sep 2015 (not shown) probably



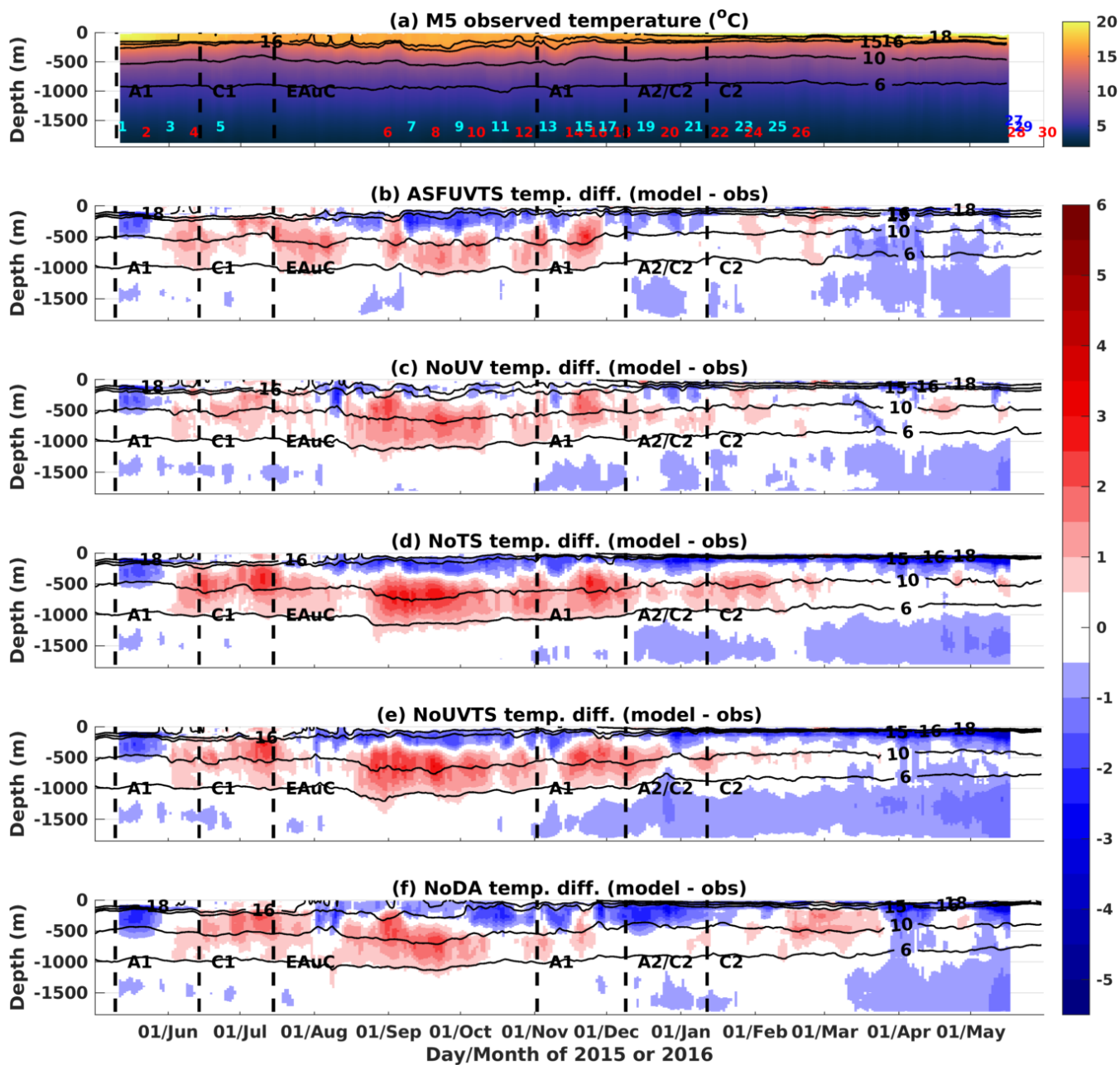


**Figure 7.** (a) M5 Observed daily average temperature and difference between modelled and observed temperature from experiments (b) ASFUVTS, (c) NoUV, (d) NoTS, (e) NoUVTS and (f) NoDA. The red, blue and cyan numbers in (a) show the dates where Argo profilers sampled the NZNES. The location of the Argo floats are shown in Fig. 1a and 8e.

due to the lack of Argo floats to the north of 35°S. ASFUVTS had the closest match to the observations out of all experiments





(Fig. 7b). In mid-Aug 2015, a near surface cold bias ( $< -2^{\circ}\text{C}$ ) was pronounced in all experiments, but further developed in the  
280 NoDA, NoTS and NoUVTS runs towards at the end of the simulation period. This is associated with the lack of subsurface  
temperature assimilation and the intrinsic variability in the model run. ASFUVTS (NoUV) run reduced the cold and warm  
differences to values below  $1^{\circ}\text{C}$  ( $2^{\circ}\text{C}$ ) for most of the period of simulation. It showed that the assimilation of temperature and  
salinity had positive impact by reducing temperature biases at M4 and M5. We did not analyse salinity results at the moorings  
due to the few number ( $\leq 3$ ) of CTDs at each station. Instead, model salinity is compared to Argo independent observations in  
285 the next section.

### 3.3 Comparison to independent observations

Thirty non-assimilated temperature and salinity profiles spread throughout the domain (Fig. 8e) and in time (Fig. 7) were used  
for model-data independent comparison. Model temperature rmsd showed similar trends to the results simulated at M4 and  
M5. When temperature was not assimilated (NoTS and NoUVTS runs) there was a higher temperature rmsd between 0 and 200  
290 m in comparison to the NoDA run due to a colder bias ( $< -1^{\circ}\text{C}$ ) that developed in those runs (blue and pink lines in Fig. 8a,b).  
Assimilation of subsurface temperature data (ASFUVTS and NoUV runs) generated smaller temperature rmsd in comparison  
to the NoDA run from near surface down to 2000 m (ASFUVTS) (1000 m in NoUV) (solid black and cyan lines in Fig. 8a,b).  
HYCOM-NCODA reanalysis which assimilates Argo, SSH and SST data had the overall best temperature representation at the  
Argo locations.

295 Comparisons to Argo measurements showed that all 7-day window experiments and the NoDA run had similar vertical  
structure in the salinity bias. Fresher salinity was modelled in the upper 200 m, and saltier waters were modelled below that,  
peaking at 600 m, in those experiments (Fig. 8c). The NoDA run had the smallest salinity rmsd from 0 to 200 m, and ASFUVTS  
had the largest at that depth (Fig. 8d). It seemed that the 8 CTD observations spread between M3-M5 were not enough to correct  
salinity in the model domain. On the other hand, ASFUVTS-2days had the smallest salinity bias and rmsd in comparison to  
300 the 7-day window experiments. It suggests that, more frequent increments to the initial conditions and doubled decorrelation  
length scales of tracers can overcome the small number of CTD observations. ASFUVTS-2days salinity results were close to  
HYCOM-NCODA reanalysis which assimilated salinity data from Argo floats.

### 3.4 Increments to initial and surface conditions

Variability in temperature increments to the initial conditions at M4 revealed oscillation between positive and negative incre-  
305 ments through time in all experiments (Fig. 9). The 7-day window experiments that assimilated subsurface temperature and  
salinity (ASFUVTS and NoUV) had positive increments extending from surface down to 500 m (Fig. 9a,b). In contrast, exper-  
iments that did not assimilate temperature and salinity (NoTS and NoUVTS) had large positive increments bounded to near  
the surface (Fig. 9c,d). ASFUVTS-2days had smaller increments throughout the water column (Fig. 9e).

Near surface average temperature increments had a distinct difference between experiments that did and did not assimilate  
310 subsurface temperature at M4 and M5 (Fig. 10a,b). Assimilation of in situ temperature (ASFUVTS and NoUV) generated  
larger average positive increments ( $> 0.04^{\circ}\text{C}$ ) in comparison to the simulations that withheld subsurface temperature (NoTS

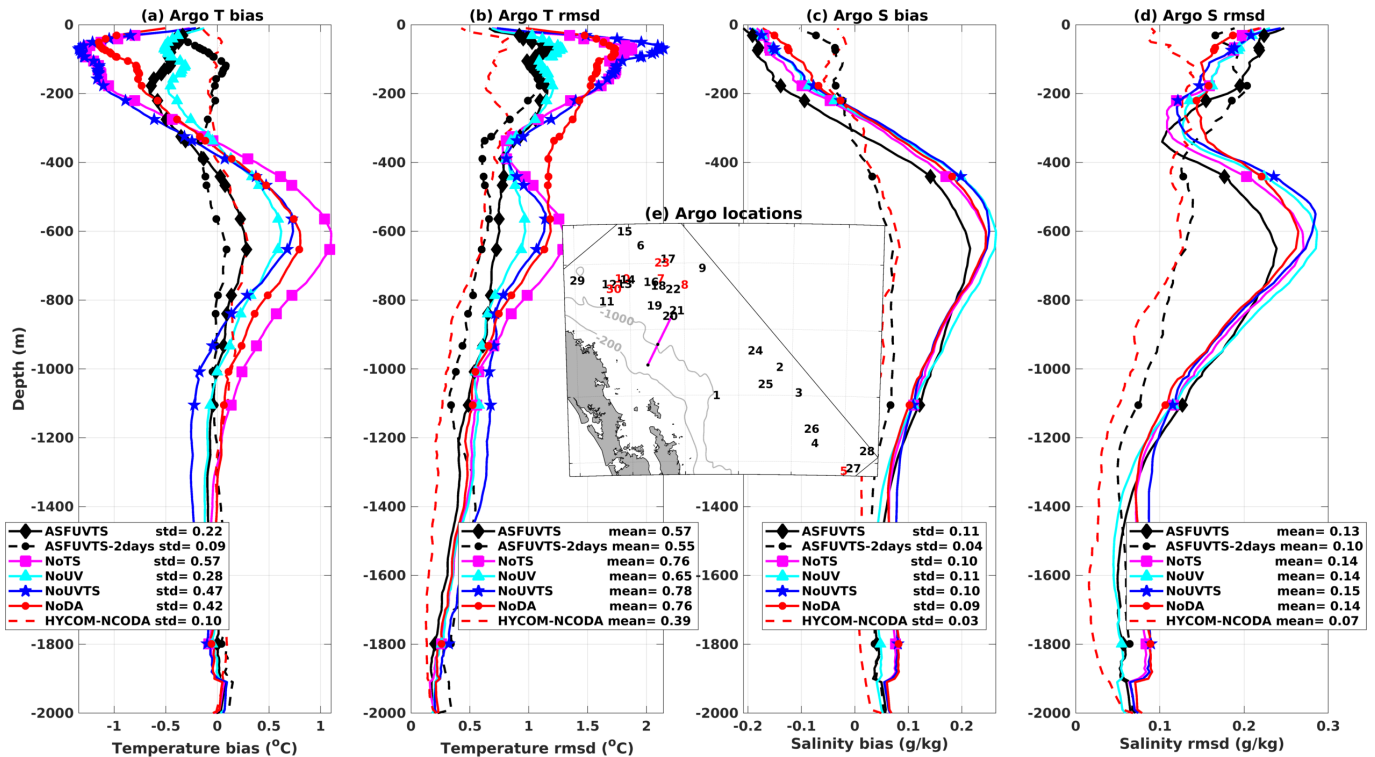


**Figure 8.** Profiles of mean bias and root mean square deviation (rmsd) between model and independent Argo observations of temperature (a,b) and salinity (c,d). Black diamonds (ASFUVTS), black dots and dashed line (ASFUVTS-2days), magenta squares (NoTS), cyan triangles (NoUV), blue stars (NoUVTS) and red dots (NoDA) represent the median depth of thermistors and CTDs (CTDs) at M3, M4 and M5 in temperature (salinity) bias and rmsd profiles. HYCOM-NCODA results are shown as dashed red lines. (e) Map of Argo locations represented as numbers in black or red for better visualisation only. The moorings' locations are shown as black dots on the magenta line.

and NoUVTS). The latter experiments had near surface mean negative temperature increments that decreased towards zero below 200 m. ASFUVTS-2days had smaller average increments throughout the water column (Fig. 10a,b).

Surface mean heat flux increments varied according to the presence/absence of subsurface temperature for assimilation (Fig. 11). Simulations that withheld subsurface temperature (NoTS and NoUVTS) had average positive increments in the majority of the domain (Fig. 11a,b). The positive heat flux increments in the NoTS and NoUVTS runs were related to the near surface negative temperature increments at M4 and M5 (dark blue and pink lines Fig. 10). The combined positive heat flux increments and negative temperature increments corrected the surface cold bias present in the NoDA run, but not the cooling trend around 200 m. Experiments that assimilated subsurface temperature (ASFUVTS, NoUV and ASFUVTS-2days) had negative average heat flux increment near the moorings that extended north and south (Fig. 11c,d,e). This negative heat flux increment might balance the positive temperature increment at M4 and M5 which aim at correcting both surface and upper thermocline (~200 m) clod biases.

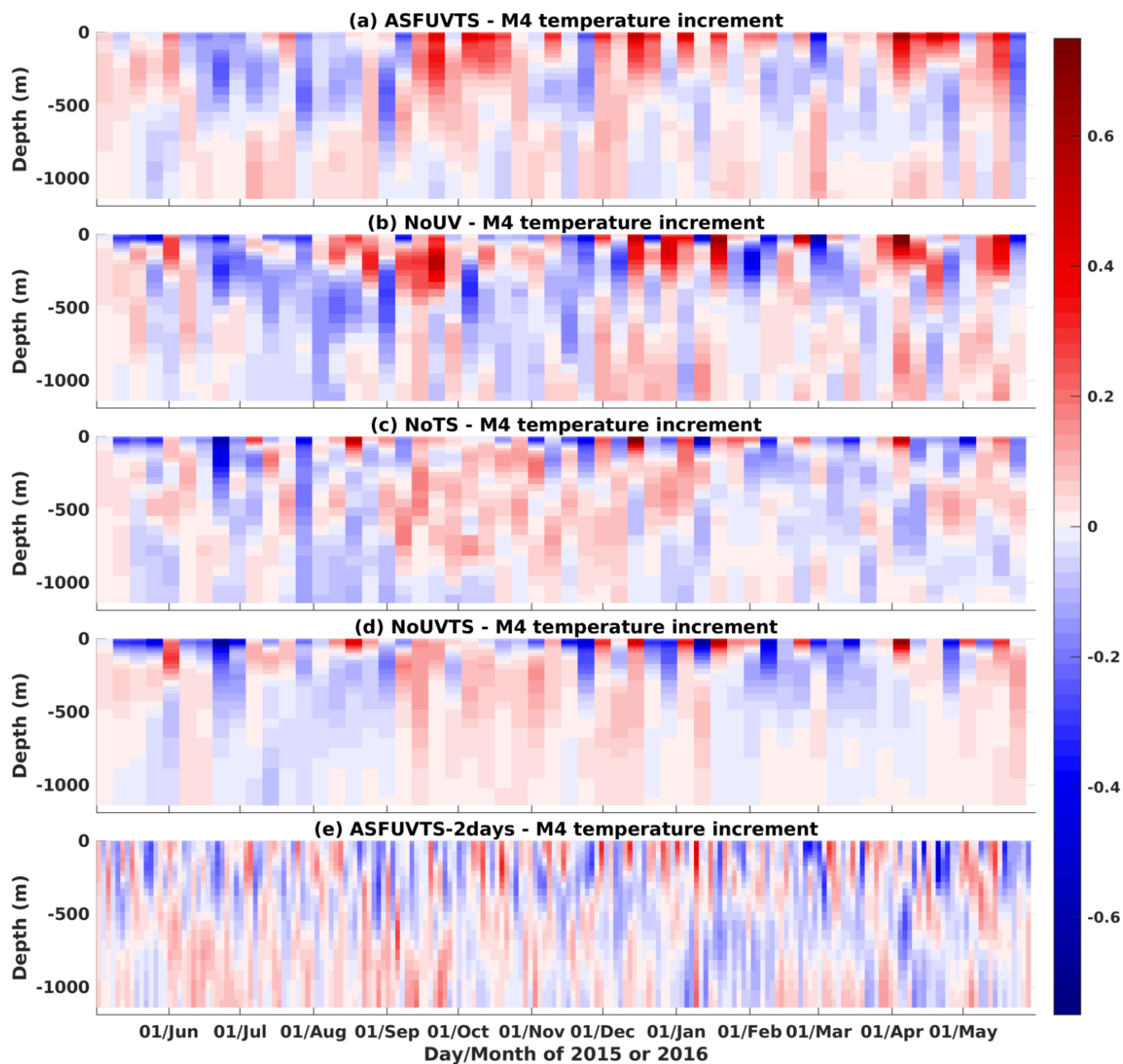


**Figure 9.** Time variability of temperature increments ( $^{\circ}\text{C}$ ) to the initial conditions at M4 from experiments (a) ASFUVTS, (b) NoUV run, (c) NoTS, (d) NoUVTS, and (e) ASFUVTS-2days.

ASFUVTS-2days run had smaller negative heat flux increments. This happened due to the smaller average negative increments (M4) and positive increments (M5) added to the initial condition of temperature at those stations (black dashed line  
325 Fig. 10). The average net heat flux showed roughly positive values north  $35^{\circ}\text{S}$  and it was negative southwards (Fig. 11f). On

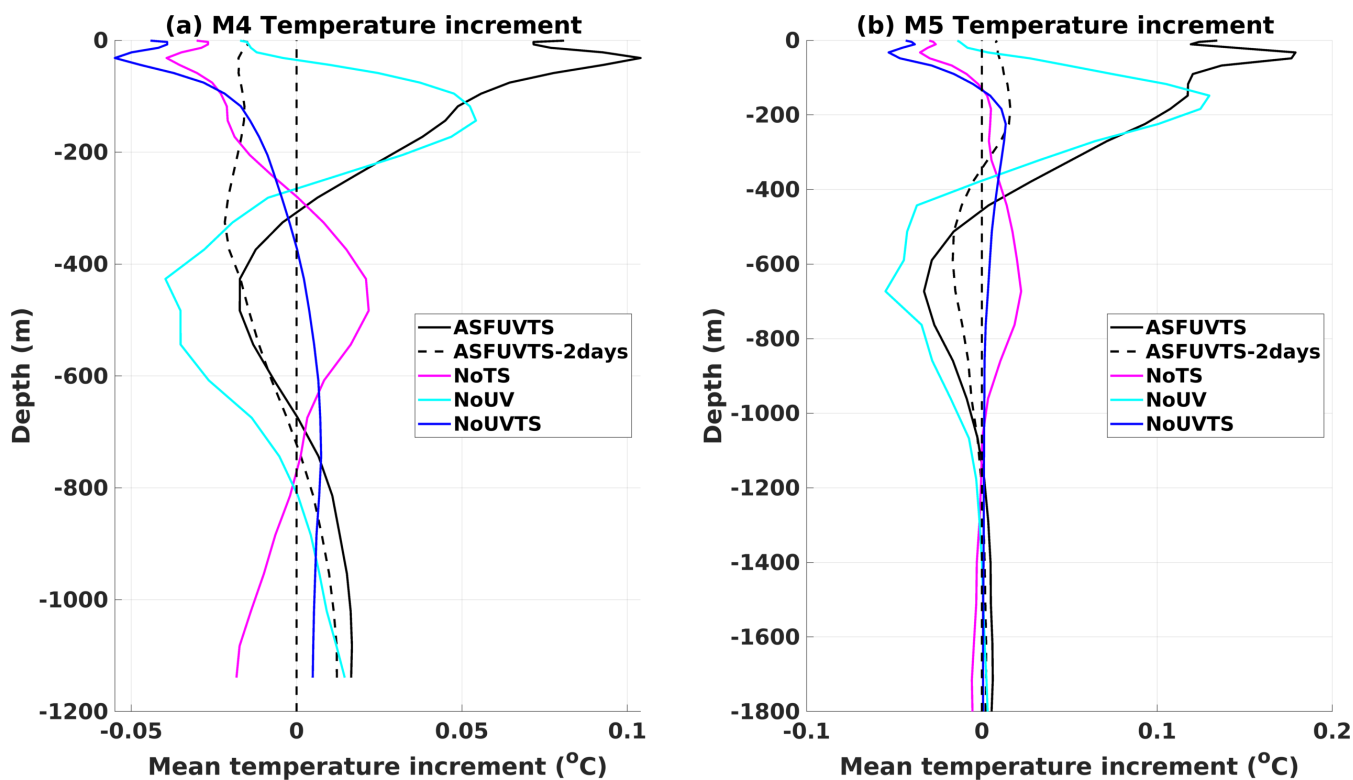


**Figure 10.** Profile of average increment to initial conditions of temperature at M4 (a) and M5 (b). Solid black line (ASFUVTS), dashed black line (ASFUVTS-2days), pink (magenta) line (NoTS), light blue (cyan) line (NoUV) and dark blue line (NoUVTS).

average, the atmosphere has warming effect on the ocean north of 35°S and cooling effect south of 35°S. This is observed in JRA55-do (Fig. 48 in Tsujino et al. (2018)), in which the NZNES is located near the average zero net heat flux contour line in the atmospheric forcing dataset.

Annual average wind stress is mainly from southwest in all experiments but wind stress curl showed some spatial variability between the assimilative runs (Fig. 12). Experiments that did not assimilate subsurface temperature and salinity (NoUVTS and NoUV) had average negative wind stress curl at the moorings' location (Fig. 12a,b). Conversely, assimilation of subsurface temperature and salinity (NoUV and ASFUVTS) generated average positive wind stress curl on top of M5 (M3-M5 in ASFUVTS) (Fig. 12c,d). Positive wind stress curl generates convergence and downwelling of warmer water masses that might be acting to prevent the cold bias in the numerical model. These changes in wind stress curl might also explain why assimilation of subsurface temperature and salinity (ASFUVTS and NoUV) slightly degraded the representation of velocity at M4 and M5 compared to withholding subsurface temperature and salinity (NoTS and NoUVTS). ASFUVTS-2days run had smaller wind stress curl magnitude compared to the other simulations. Its wind stress curl field resembles the NoDA wind field forced with JRA55-do, especially in the regions of negative wind stress curl near the coast around 37.5°S and observed by Taboada et al. (2019) using CCMP data.

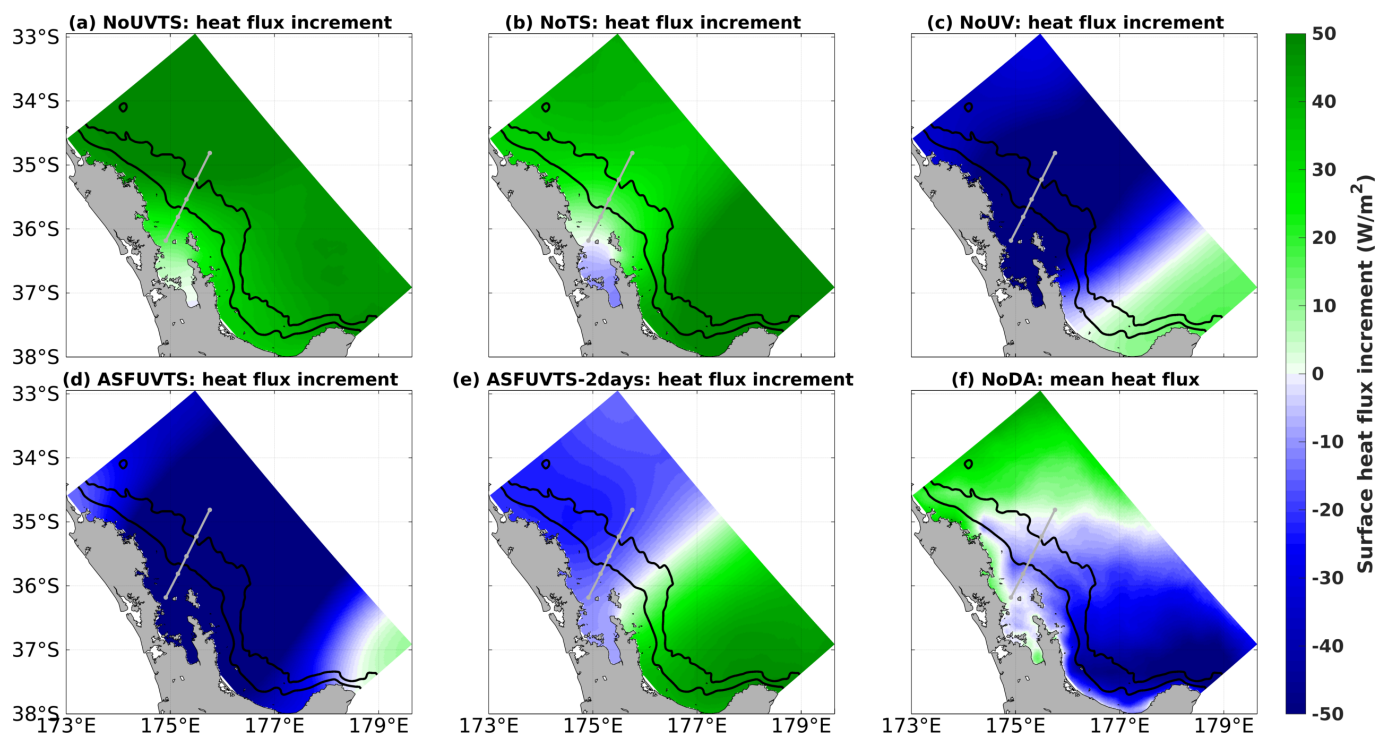


**Figure 11.** Average surface heat flux increments ( $\text{W/m}^2$ ) (positive = downward) in experiments (a) NoUVTS, (b) NoTS, (c) NoUV, (d) ASFUVTS, and (e) ASFUVTS-2days. (f) shows mean net heat flux in the freely evolving simulation (NoDA). Green (blue) colours show positive (negative) mean surface heat flux.

#### 340 4 Discussion and comparison to other studies

In this study, SSH, SST, mooring velocity, temperature and salinity observations were assimilated into an ocean model of the EAUC using 4D-Var with a 7-day window length. Observing system experiments (OSEs) were conducted in order to elucidate the importance of in situ data assimilation in the EAUC region. 4 OSEs were performed based on the most complete simulation called ASFUVTS which assimilated surface fields (SSH and SST), and mooring velocity, temperature and salinity. The other  
345 experiments withheld observation types from assimilation. They removed mooring velocities (NoUV); subsurface temperature and salinity (NoTS); and all mooring data (NoUVTS). A non-assimilative freely evolving simulation (NoDA) was used as the control. Argo data was left out of all experiments for independent model-data comparison. Another run that assimilated surface and mooring data using a 4D-Var 2-day window (ASFUVTS-2days) and HYCOM-NCODA were also used in the model comparison.

350 All assimilative experiments showed a reduction in SSH rmsd in comparison to the NoDA run of about 25%. The improvements in SSH were small in comparison to achievements seen in other WBC 4D-Var studies, such as: the East Australian Current (EAC) (~63% Kerry et al. (2016)) and the Brazil Current (BC) (48% - de Paula et al. (2021)). Smaller correction in

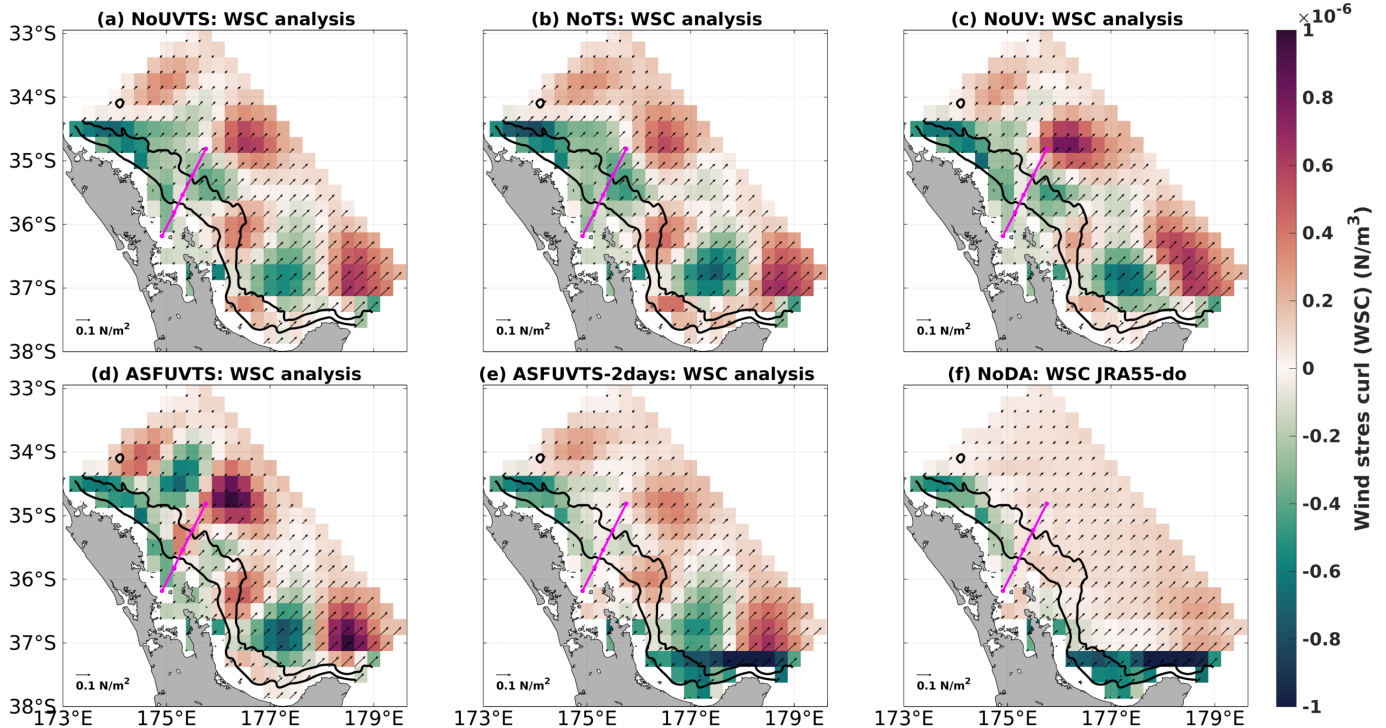


**Figure 12.** Analysis field of wind stress ( $\text{N/m}^2$ ) and its curl ( $\text{N/m}^3$ ) (red-green shade) in experiments (a) NoUVTS, (b) NoTS, (c) NoUV, (d) ASFUVTS, and (e) ASFUVTS-2days. (f) shows mean wind stress and its curl from JRA55-do. All fields were degraded from 2 km to  $1/4^\circ$  to be similar to JRA55-do horizontal resolution.

SST (rmsd reduction of 37%) when compared to 4D-Var studies in the East Australian Current (EAC) ( $\sim 60\%$  Kerry et al. (2016)) and the Brazil Current (BC) (27% - de Paula et al. (2021)). These studies used lower horizontal resolution grids in  
355 open ocean (5 km EAC and 9 km BC) compared to our model spatial grid spacing (2 km) which might explain the differences in performance. According to Sandery and Sakov (2017), increasing model resolution towards the submesoscale (from 10 km to 2.5 km) reduces the skill of the analysis and forecast generated. They suggested that resolving the less predictable submesoscale lowers the predictability of the mesoscale as there is an inverse cascade in the kinetic energy spectrum. Kerry et al. (2020) found larger errors when downscaling from a regional to a coastal domain (750-1000 m resolution) while simulating  
360 the cyclonic inshore side and frontal instabilities of the EAC.

All OSEs improved velocity complex correlation by at least 3-fold at M4 and 5-fold at M5 in comparison to the NoDA run (coef.  $< 0.07$ ). Including velocities in the assimilation (NoTS) improved on the simulation which only assimilated surface fields (NoUVTS). This was most notable at M4, where the velocity data assists the model in better capturing frequent reverse flows at depth. Counterintuitively, inclusion of temperature and salinity (NoUV and ASFUVTS) degraded the velocity results  
365 in comparison to NoUVTS run. This might be associated with the low vertical resolution of salinity sensors, which were not enough to correct density fields and generate accurate geostrophic currents. For future data collection strategies, we suggest





that higher vertical resolution for salinity data. Changes in the wind stress curl analysis field had a negative impact in the representation of the velocity at M4 and M5 and may be the main cause for that. Larger positive wind stress curl was generated near the moorings in ASFUVTS and NoUV runs. Positive wind stress curl causes downwelling of warmer waters and counter-  
370 balances the cold bias in the model but degraded velocity results in ASFUVTS and NoUV runs.

The 2-day assimilation window run (ASFUVTS-2days) showed the highest complex correlation coefficients ( $>0.35$ ) which combined doubled decorrelation length scales, larger model error estimate and more frequent increments. ASFUVTS-2days overcame the low vertical resolution of salinity and temperature observations and generated the best results when compared to Argo distant locations. However, this approach must be used with care if subsurface data availability is low because larger  
375 colder biases can be generated. In Kerry et al. (2016), higher velocity complex correlation coefficients ( $\sim 1$ ) were obtained in a 2-year reanalysis of the EAC. However, the EAC has a more coherent jet (Mata et al., 2000; Bowen et al., 2005; Sloyan et al., 2016) which is well represented by the non-assimilative run (complex correlation  $\sim 0.8$  in some locations) (Kerry et al., 2016). In contrast, the EAuC has a more eddy-dominated field (2/3 of 1 year) (Santana et al., 2021) which makes it harder for ocean free-running models and reanalyses to capture such variability.

380 Marked differences between the experiments arose when model results were compared to subsurface observations of temperature. Experiments that withheld in situ temperature and salinity (NoTS and NoUVTS) generated a larger cold bias around 100 m at M4 and M5 in comparison to the NoDA run. At 100 m, errors were about  $1.4^{\circ}\text{C}$  ( $1.9^{\circ}\text{C}$ ) in the NoTS (NoUVTS) run at M4 and M5, whereas the NoDA run had temperature rmsd of  $1.1^{\circ}\text{C}$  ( $1.6^{\circ}\text{C}$ ) at M4 (M5). Assimilation of in situ temperature and salinity (ASFUVTS and NoUV) prevented that and had improved results against the NoDA run. The lack of subsurface  
385 temperature assimilation also generated similar errors at the top of the thermocline in other regional studies (e.g., Zavala-Garay et al. (2012); Santana et al. (2020)). Zavala-Garay et al. (2012) needed to assimilate XBT or synthetic CTD data to correct that large temperature rmsd ( $\sim 2^{\circ}\text{C}$ ) between 200 and 500 m depth. The authors aimed at simulating the EAC variability between years 2001 and 2002, and the Argo project was still beginning, with few sondes in the ocean. In our study, comparisons to HYCOM-NCODA suggest that assimilating the few Argo temperature and salinity profiles (30) and surface data could prevent  
390 the growth of the 100 m cold bias at M4 and M5. However, it still an open question if this would improve the ROMS 4D-Var results used in this study. These experiments represent a good benchmark to define proper assimilation window and decorrelation length scales. Doubled length scales of tracers (200 km and 200 m) and a 2-day assimilation window led to colder biases in the experiments that withheld in situ temperature (not shown) which could be a problem when Argo data is not available for a long period. The 7-day assimilation window and smaller length scales (100 km and 100 m) seem to be a good configuration  
395 to well-represent the surface (SSH and SST) and subsurface velocity fields in case of application in an operational forecast system.

Model temperature comparisons to Argo data showed similar results to those simulated at M4 and M5. NoTS and NoUVTS runs had a larger cold bias near 100 m depth which generated a higher temperature rmsd ( $\sim 2^{\circ}\text{C}$ ) in comparison to the NoDA run ( $\sim 1.6^{\circ}\text{C}$ ). A warm bias was also evident around 600 m, in all experiments with varying degrees. Assimilation of mooring  
400 temperature (ASFUVTS and NoUV) reduced the cold bias and the temperature rmsd ( $\sim 1^{\circ}\text{C}$ ) in comparison to the NoDA run. The shallow-cold and deeper-warm biases are intrinsic to the NoDA run, which might be associated with biases in the boundary



condition from HYCOM-NCODA when Argo data was not available (between Jun and Sep 2015) for assimilation north of 35°S. Even though larger temperature errors were observed in the simulations that withheld mooring temperature and salinity (1.6 - 2.1°C), they were still comparable to freely evolving simulations temperature rmsd ( $\sim 1.9^\circ\text{C}$ ) in other studies (e.g., Kerry et al. (2016); Siripatana et al. (2020)) when assessed using Argo temperature.

Data assimilation of subsurface observations using a 7-day window and smaller decorrelation length scales had little impact in correcting salinity at the Argo locations. A small salinity degradation was simulated between 0 and 200 m in the assimilative experiments in comparison to the NoDA run. Negative impact on near surface salinity was also observed when assimilating SST or SSH data only in the Brazil Current region (Santana et al., 2020). Some authors suggest that assimilation of salinity data is needed to constrain the model water column salinity (e.g., Oke and Schiller (2007); Tanajura et al. (2014); Oke et al. (2015)). Assimilation of surface and subsurface data every 2 days with larger decorrelation length scale of tracers (ASFUVTS-2days) was able to considerably correct model salinity below 400 m in relation to the NoDA run. ASFUVTS-2days run reached error values similar to HYCOM-NCODA which assimilated salinity data from Argo floats.

Increments to temperature initial conditions were positive and deep (200 m) in the experiments that assimilated subsurface temperature (ASUVTS and NoUV). In contrast, withholding in situ temperature (NoTS and NoUVTS) generated negative and shallower (50 m) increments. This generated differences in the atmospheric heat fluxes, where NoTS and NoUVTS had average positive heat flux increment in most of the domain to compensate the negative increments to the temperature initial condition. The combined positive heat flux increments and negative temperature increments corrected the surface cold bias present in the NoDA run, but not the cooling trend around 200 m. Conversely, experiments that assimilated subsurface temperature (ASFUVTS and NoUV) had negative average heat flux increment near the moorings. This negative heat flux increment balanced the positive temperature increment at M4 and M5 which aimed at correcting both surface and upper thermocline ( $\sim 200$  m) cold biases.

ASFUVTS, NoUV and ASFUVTS-2days runs (assimilated subsurface temperature) had net heat flux increment varying from negative (near the moorings and north of the domain) to positive flux in the southeast region of the model domain. This variability might be associated with the heat flux that forced the NoDA run. It was positive north of 35°S and negative southwards. The NZNES is located near the zero heat flux line in JRA55-do atmospheric forcing used in this study (Fig. 48 in Tsujino et al. (2018)). For instance, the Hawaiian archipelago is also located near a zero line heat flux in the atmospheric forcing product. 4D-Var experiments in the region, also showed large average heat flux increments ( $\pm 100 \text{ W/m}^2$ ), and marked spatial variability with negative increments in the lee of the islands and positive increments to the west of that (Matthews et al., 2012).

Positive wind stress curl was generated on top of M5 when subsurface temperature data was assimilated (ASFUVTS and NoUV). Positive wind stress curl generates convergence and downwelling of warmer waters which might be associated with corrections of the 200 m cold bias. Positive wind stress curl correction was also observed in the simulations on SE Brazil which reduced the magnitude of upwelling in the region (de Paula et al., 2021). Changes in the wind stress curl in ASFUVTS and NoUV runs (assimilated subsurface temperature) were also responsible to the lowered velocity complex correlation at M4 and M5 in comparison to the simulations that withheld subsurface temperature. If more subsurface salinity data were available,



the solutions ASFUVTS and NoUV runs could have converged to improved density structures that resulted in better simulated currents as we observed in ASFUVTS-2days.

## 5 Conclusions and future work

440 By running the OSEs we elucidate the importance of different datasets on the quality of ocean reanalyses. The representation of surface fields and consequent mesoscale eddies was improved by data assimilation of surface data only. The model high spatial resolution (2 km) which starts to solve submesoscale variability might be responsible for the lower skill compared to other 4D-Var regional studies that had lower horizontal resolution ( $> 5$  km). In situ subsurface temperature is of utmost importance to correctly simulate the top of the thermocline - one of the most difficult regions to simulate in ocean models.

445 The lack of subsurface temperature for assimilation (NoTS and NoUVTS) increased the near surface cold bias present in the freely evolving model run (NoDA). Assimilation of mooring temperature (ASFUVTS and NoUV) corrects this, even at distant Argo locations. Data assimilation using a 2-day window and doubled decorrelation length scales better matched the assimilated and independent observations. This approach must be used with care if subsurface data availability is low (e.g., using Argo floats only as subsurface data) because larger cold bias in the upper-thermocline can be generated (not shown). Nevertheless,

450 all reanalyses showed improved velocity results on the mid-slope when compared to HYCOM-NCODA, which shows the importance of downscaling to better represent the slope bathymetry and possibly shelf-slope exchange.

The current work is part of a set of experiments that prepare for a data assimilative ocean forecast for the NZNES. New experiments based on the 7-day window configuration can be conducted using Argo and glider data. Questions regarding the absence or presence of glider data can be asked and the impact on the velocity field evaluated with observations. Continuous

455 temperature and salinity sampling from ocean gliders would provide enough high vertical resolution and good spatial coverage that would positively impact the simulation of the thermohaline field and ocean currents.

In the future, a posterior check of the consistency of the observation and background error hypotheses (Mattern et al., 2018) can be applied to improve the quality of the ocean reanalyses. Mattern et al. (2018) described how the covariance of residuals and innovations, and the covariance of increments and innovations, should be roughly equal to the assumed observation and background error variances, respectively. Posterior tests of these statistics probe whether the prior assumptions for error vari-

460 ances need adjusting to be consistent with the model intrinsic skill and representativeness error. This method has been applied to the Mercator-Ocean forecast system (GLORYS) to obtain better performance (Lellouche et al., 2018). Moreover, an Ensemble 4D-Var approach can be applied to improve the quality of the analysis on the NZNES. This methodology uses several perturbed simulations (Ensemble) to estimate the model error covariance matrix ( $\mathbf{D}$ ) (e.g., Pasmans and Kurapov (2019)). This

465 includes spatial and temporal variability to  $\mathbf{D}$  compared to a fixed model covariance matrix used here. This method showed improved representation of glider temperature and salinity observations when compared to 4D-Var using a static  $\mathbf{D}$  (Pasmans et al., 2020).



*Code availability.* The Regional Ocean Model System (ROMS) is widely known in the modelling oceanographic community and its source code, documentation, and discussion forum can be found at <https://www.myroms.org/>. Configuration files and scripts for analysing model output can be found on <https://doi.org/10.5281/zenodo.7306271>

*Author contributions.* J.O. conducted the sampling experiment. H.M. set up the numerical model and lateral conditions. R.S. analysed the data, included new atmospheric forcing in the model, generated the data assimilative runs, analysed the results and wrote the manuscript. B.P. supervised the improvement of the reanalysis and provided seapy (python library for ocean state estimate). R.S., H.M., J.O., B.P., S.W., and S.S. discussed the results and reviewed the manuscript.

475 *Competing interests.* No competing interests are present

*Acknowledgements.* We thank everyone involved in data collection and curation at NIWA, as well as support from the New Zealand eScience Infrastructure (NeSI) that made this work possible. Funding was provided by NIWA Strategic Science Investment Fund (SSIF) Ocean-Climate Interactions Programme, and Flows and Productivity Programme and MBIE endeavour Smart idea grant CO1X1814. We also thank John Wilkin who provided extra comments that improved the manuscript.



## 480 References

- Bowen, M. M., Wilkin, J. L., and Emery, W. J.: Variability and forcing of the East Australian Current, *Journal of Geophysical Research: Oceans*, 110, <https://doi.org/10.1029/2004JC002533>, 2005.
- Casey, K. S., Brandon, T. B., Cornillon, P., and Evans, R.: The Past, Present, and Future of the AVHRR Pathfinder SST Program, pp. 273–287, Springer Netherlands, Dordrecht, [https://doi.org/10.1007/978-90-481-8681-5\\_16](https://doi.org/10.1007/978-90-481-8681-5_16), 2010.
- 485 Chapman, D. C.: Numerical treatment of cross-shelf open boundaries in a barotropic coastal ocean model, *Journal of Physical oceanography*, 15, 1060–1075, 1985.
- Chassignet, E. P., Hurlburt, H. E., Metzger, E. J., Smedstad, O. M., Cummings, J. A., Halliwell, G. R., Bleck, R., Baraille, R., Wallcraft, A. J., Lozano, C., et al.: US GODAE: global ocean prediction with the HYbrid Coordinate Ocean Model (HYCOM), *Oceanography*, 22, 64–75, 2009.
- 490 Chiswell, S. M.: Determining the internal structure of the ocean off northeast New Zealand from surface measurements, *New Zealand Journal of Marine and Freshwater Research*, 35, 289–306, <https://doi.org/10.1080/00288330.2001.9516999>, publisher: Taylor & Francis, 2001.
- de Paula, T. P., Lima, J. A. M., Tanajura, C. A. S., Andrioni, M., Martins, R. P., and Arruda, W. Z.: The impact of ocean data assimilation on the simulation of mesoscale eddies at Sao Paulo plateau (Brazil) using the regional ocean modeling system, *Ocean Modelling*, 167, 101 889, <https://doi.org/https://doi.org/10.1016/j.ocemod.2021.101889>, 2021.
- 495 de Souza, J. M. A. C., Powell, B., Castillo-Trujillo, A. C., and Flament, P.: The vorticity balance of the ocean surface in Hawaii from a regional reanalysis, *Journal of Physical Oceanography*, 45, 424–440, 2015.
- de Souza, J. M. A. C., Couto, P., Soutelino, R., and Roughan, M.: Evaluation of four global ocean reanalysis products for New Zealand waters—A guide for regional ocean modelling, *New Zealand Journal of Marine and Freshwater Research*, 55, 132–155, 2021.
- Di Lorenzo, E., Moore, A. M., Arango, H. G., Cornuelle, B. D., Miller, A. J., Powell, B., Chua, B. S., and Bennett, A. F.: Weak and strong  
500 constraint data assimilation in the inverse Regional Ocean Modeling System (ROMS): Development and application for a baroclinic coastal upwelling system, *Ocean Modelling*, 16, 160–187, 2007.
- Ducet, N., Le Traon, P. Y., and Reverdin, G.: Global high-resolution mapping of ocean circulation from TOPEX/Poseidon and ERS-1 and -2, *Journal of Geophysical Research: Oceans*, 105, 19 477–19 498, <https://doi.org/https://doi.org/10.1029/2000JC900063>, 2000.
- Fairall, C. W., Bradley, E. F., Hare, J., Grachev, A. A., and Edson, J. B.: Bulk parameterization of air–sea fluxes: Updates and verification for  
505 the COARE algorithm, *Journal of climate*, 16, 571–591, 2003.
- Feng, M., Wijffels, S., Godfrey, S., and Meyers, G.: Do eddies play a role in the momentum balance of the Leeuwin Current?, *Journal of Physical Oceanography*, 35, 964–975, 2005.
- Fisher, M. and Courtier, P.: Estimating the covariance matrices of analysis and forecast error in variational data assimilation, *ECMWF Tech. Mem.* 220, 1995.
- 510 Haidvogel, D. B., Arango, H., Budgell, W. P., Cornuelle, B. D., Curchitser, E., Di Lorenzo, E., Fennel, K., Geyer, W. R., Hermann, A. J., Lanerolle, L., et al.: Ocean forecasting in terrain-following coordinates: Formulation and skill assessment of the Regional Ocean Modeling System, *Journal of computational physics*, 227, 3595–3624, 2008.
- Janeković, I., Mihanović, H., Vilibić, I., Grčić, B., Ivatek-Šahdan, S., Tudor, M., and Djakovac, T.: Using multi-platform 4D-Var data assimilation to improve modeling of Adriatic Sea dynamics, *Ocean Modelling*, 146, 101 538, 2020.



- 515 Kerry, C., Powell, B., Roughan, M., and Oke, P.: Development and evaluation of a high-resolution reanalysis of the East Australian Current region using the Regional Ocean Modelling System (ROMS 3.4) and Incremental Strong-Constraint 4-Dimensional Variational (IS4D-Var) data assimilation, *Geoscientific Model Development*, 9, 3779–3801, 2016.
- Kerry, C., Roughan, M., and Powell, B.: Predicting the submesoscale circulation inshore of the East Australian Current, *Journal of Marine Systems*, 204, 103 286, 2020.
- 520 Kundu, P. K.: Ekman Veering Observed near the Ocean Bottom, *Journal of Physical Oceanography*, 6, 238 – 242, [https://doi.org/10.1175/1520-0485\(1976\)006<0238:EVONTO>2.0.CO;2](https://doi.org/10.1175/1520-0485(1976)006<0238:EVONTO>2.0.CO;2), 1976.
- Laing, A. K., Oien, N. A., Murphy, R., and Uddstrom, M. J.: Coherent signals in the temperature and height of the sea surface off North Cape, New Zealand, *New Zealand Journal of Marine and Freshwater Research*, 32, 187–202, <https://doi.org/10.1080/00288330.1998.9516819>, 1998.
- 525 Lellouche, J.-M., Greiner, E., Le Galloudec, O., Regnier, C., Benkiran, M., Testut, C.-E., Bourdalle-Badie, R., Drevillon, M., Garric, G., and Drillet, Y.: Mercator Ocean Global High-Resolution Monitoring and Forecasting System, *New Frontiers in Operational Oceanography*, pp. 563–592, 2018.
- Levin, J., Arango, H. G., Laughlin, B., Hunter, E., Wilkin, J., and Moore, A. M.: Observation impacts on the Mid-Atlantic Bight front and cross-shelf transport in 4D-Var ocean state estimates: Part I—Multiplatform analysis, *Ocean Modelling*, 156, 101 721, 2020.
- 530 López, A. G., Wilkin, J. L., and Levin, J. C.: Doppio—a ROMS (v3. 6)-based circulation model for the Mid-Atlantic Bight and Gulf of Maine: configuration and comparison to integrated coastal observing network observations, *Geoscientific Model Development*, 13, 3709–3729, 2020.
- Marchesiello, P., McWilliams, J. C., and Shchepetkin, A.: Open boundary conditions for long-term integration of regional oceanic models, *Ocean modelling*, 3, 1–20, 2001.
- 535 Marchesiello, P., McWilliams, J. C., and Shchepetkin, A.: Equilibrium structure and dynamics of the California Current System, *Journal of physical Oceanography*, 33, 753–783, 2003.
- Mason, E., Molemaker, J., Shchepetkin, A. F., Colas, F., McWilliams, J. C., and Sangrà, P.: Procedures for offline grid nesting in regional ocean models, *Ocean Modelling*, 35, 1–15, <https://doi.org/https://doi.org/10.1016/j.ocemod.2010.05.007>, 2010.
- Mata, M. M., Tomczak, M., Wijffels, S., and Church, J. A.: East Australian Current volume transports at 30°S: Estimates from the World  
540 Ocean Circulation Experiment hydrographic sections PR11/P6 and the PCM3 current meter array, *Journal of Geophysical Research: Oceans*, 105, 28 509–28 526, <https://doi.org/10.1029/1999JC000121>, 2000.
- Mattern, J. P., Edwards, C. A., and Moore, A. M.: Improving variational data assimilation through background and observation error adjustments, *Monthly Weather Review*, 146, 485–501, 2018.
- Matthews, D., Powell, B., and Janeković, I.: Analysis of four-dimensional variational state estimation of the Hawaiian waters, *Journal of  
545 Geophysical Research: Oceans*, 117, 2012.
- Mazloff, M. R., Heimbach, P., and Wunsch, C.: An eddy-permitting Southern Ocean state estimate, *Journal of Physical Oceanography*, 40, 880–899, 2010.
- Moore, A., Arango, Hernanand Broquet, G., Veneziani, M., Edwards, C., Powell, B., Foley, D., Doyle, J. D., Costa, D., and Robinson, P.: The  
550 Regional Ocean Modeling System (ROMS) 4-dimensional variational data assimilation systems: Part II - Performance and application to the California Current System, *Progress in Oceanography*, 91, 50–73, 2011a.





- Moore, A. M., Arango, H. G., Broquet, G., Powell, B. S., Weaver, A. T., and Zavala-Garay, J.: The Regional Ocean Modeling System (ROMS) 4-dimensional variational data assimilation systems: Part I–System overview and formulation, *Progress in Oceanography*, 91, 34–49, 2011b.
- Moore, A. M., Levin, J., Arango, H. G., and Wilkin, J.: Assessing the performance of an ocean observing, analysis and forecast System for the Mid-Atlantic Bight using array modes, *Ocean Modelling*, 164, 101 821, 2021.
- 555 O’Callaghan, J., Mike, B., and Fiona, E.: Across-shelf mooring array from the northeast shelf of New Zealand, SEANOE, <https://doi.org/https://doi.org/10.17882/78971>, 2015.
- Oke, P., Schiller, A., Griffin, D., and Brassington, G.: Ensemble data assimilation for an eddy-resolving ocean model of the Australian region, *Quarterly Journal of the Royal Meteorological Society: A journal of the atmospheric sciences, applied meteorology and physical oceanography*, 131, 3301–3311, 2005.
- 560 Oke, P. R. and Schiller, A.: Impact of Argo, SST, and altimeter data on an eddy-resolving ocean reanalysis, *Geophysical Research Letters*, 34, 2007.
- Oke, P. R., Sakov, P., Cahill, M. L., Dunn, J. R., Fiedler, R., Griffin, D. A., Mansbridge, J. V., Ridgway, K. R., and Schiller, A.: Towards a dynamically balanced eddy-resolving ocean reanalysis: BRAN3, *Ocean Modelling*, 67, 52–70, 2013.
- 565 Oke, P. R., Larnicol, G., Fujii, Y., Smith, G. C., Lea, D. J., Guinehut, S., Remy, E., Balmaseda, M. A., Rykova, T., Surcel-Colan, D., et al.: Assessing the impact of observations on ocean forecasts and reanalyses: Part 1, Global studies, *Journal of Operational Oceanography*, 8, s49–s62, 2015.
- Oke, P. R., Roughan, M., Cetina-Heredia, P., Pilo, G. S., Ridgway, K. R., Rykova, T., Archer, M. R., Coleman, R. C., Kerry, C. G., Rocha, C., et al.: Revisiting the circulation of the East Australian Current: Its path, separation, and eddy field, *Progress in Oceanography*, 176, 102 139, 2019.
- 570 Osafune, S., Masuda, S., Sugiura, N., and Doi, T.: Evaluation of the applicability of the Estimated State of the Global Ocean for Climate Research (ESTOC) data set, *Geophysical Research Letters*, 42, 4903–4911, 2015.
- Pasmans, I. and Kurapov, A. L.: Ensemble of 4DVARs (En4DVar) data assimilation in a coastal ocean circulation model, part I: methodology and ensemble statistics, *Ocean Modelling*, 144, 101 493, 2019.
- 575 Pasmans, I., Kurapov, A., Barth, J., Ignatov, A., Kosro, P., and Shearman, R.: Why Gliders Appreciate Good Company: Glider Assimilation in the Oregon-Washington Coastal Ocean 4DVAR System With and Without Surface Observations, *Journal of Geophysical Research: Oceans*, 124, 750–772, 2019.
- Pasmans, I., Kurapov, A. L., Barth, J. A., Kosro, P. M., and Shearman, R. K.: Ensemble 4DVAR (En4DVar) data assimilation in a coastal ocean circulation model. Part II: Implementation offshore Oregon-Washington, USA, *Ocean Modelling*, 154, 101 681, 2020.
- 580 Phillipson, L. and Toumi, R.: Impact of data assimilation on ocean current forecasts in the Angola Basin, *Ocean Modelling*, 114, 45–58, 2017.
- Powell, B.: Quantifying how observations inform a numerical reanalysis of Hawaii, *Journal of Geophysical Research: Oceans*, 122, 8427–8444, 2017.
- Powell, B., Arango, H., Moore, A., Di Lorenzo, E., Milliff, R., and Foley, D.: 4DVAR data assimilation in the intra-Americas sea with the Regional Ocean Modeling System (ROMS), *Ocean Modelling*, 23, 130–145, 2008.
- 585 Roemmich, D. and Sutton, P.: The mean and variability of ocean circulation past northern New Zealand: Determining the representativeness of hydrographic climatologies, *Journal of Geophysical Research: Oceans*, 103, 13 041–13 054, <https://doi.org/10.1029/98JC00583>, 1998.



- Roemmich, D., Alford, M. H., Claustre, H., Johnson, K., King, B., Moum, J., Oke, P., Owens, W. B., Pouliquen, S., Purkey, S., et al.: On the future of Argo: A global, full-depth, multi-disciplinary array, *Frontiers in Marine Science*, 6, 439, 2019.
- 590 Sandery, P. A. and Sakov, P.: Ocean forecasting of mesoscale features can deteriorate by increasing model resolution towards the submesoscale, *Nature communications*, 8, 1–8, 2017.
- Santana, R., Costa, F. B., Mignac, D., Santana, A. N., Vidal, V. F. d. S., Zhu, J., and Tanajura, C. A. S.: Model sensitivity experiments on data assimilation, downscaling and tides for the representation of the Cape São Tomé Eddies, *Ocean Dynamics*, 70, 77–94, <https://doi.org/10.1007/s10236-019-01307-w>, 2020.
- 595 Santana, R., Suanda, S., Macdonald, H., and O’Callaghan, J.: Mesoscale and wind-driven intra-annual variability in the East Auckland Current, *Scientific Reports*, 9764, <https://doi.org/https://doi.org/10.1038/s41598-021-89222-3>, 2021.
- Shchepetkin, A. F. and McWilliams, J. C.: A method for computing horizontal pressure-gradient force in an oceanic model with a nonaligned vertical coordinate, *Journal of Geophysical Research: Oceans*, 108, 2003.
- Shchepetkin, A. F. and McWilliams, J. C.: The regional oceanic modeling system (ROMS): a split-explicit, free-surface, topography-  
600 following-coordinate oceanic model, *Ocean Modelling*, 9, 347–404, 2005.
- Shchepetkin, A. F. and McWilliams, J. C.: Computational kernel algorithms for fine-scale, multiprocess, longtime oceanic simulations, in: *Handbook of Numerical Analysis*, vol. 14, pp. 121–183, Elsevier, 2009.
- Siripatana, A., Kerry, C., Roughan, M., Souza, J. M. A. C., and Keating, S.: Assessing the Impact of Nontraditional Ocean Observations for Prediction of the East Australian Current, *Journal of Geophysical Research: Oceans*, 125, e2020JC016580, <https://doi.org/https://doi.org/10.1029/2020JC016580>, e2020JC016580 2020JC016580, 2020.
- 605 Sloyan, B. M., Ridgway, K. R., and Cowley, R.: The East Australian Current and Property Transport at 27°S from 2012 to 2013, *Journal of Physical Oceanography*, 46, 993–1008, <https://doi.org/10.1175/JPO-D-15-0052.1>, 2016.
- Stanton, B. and Sutton, P.: Velocity measurements in the East Auckland Current northeast of North Cape, New Zealand, *New Zealand Journal of Marine and Freshwater Research*, 37, 195–204, <https://doi.org/10.1080/00288330.2003.9517157>, 2003.
- 610 Stanton, B. R. and Morris, M. Y.: Direct velocity measurements in the Subantarctic Front and over Campbell Plateau, southeast of New Zealand, *Journal of Geophysical Research: Oceans*, 109, <https://doi.org/https://doi.org/10.1029/2002JC001339>, 2004.
- Stanton, B. R., Sutton, P. J. H., and Chiswell, S. M.: The East Auckland Current, 1994–95, *New Zealand Journal of Marine and Freshwater Research*, 31, 537–549, <https://doi.org/10.1080/00288330.1997.9516787>, 1997.
- Taboada, F. G., Stock, C. A., Griffies, S. M., Dunne, J., John, J. G., Small, R. J., and Tsujino, H.: Surface winds from  
615 atmospheric reanalysis lead to contrasting oceanic forcing and coastal upwelling patterns, *Ocean Modelling*, 133, 79–111, <https://doi.org/https://doi.org/10.1016/j.ocemod.2018.11.003>, 2019.
- Tanajura, C., Novaes Santana, A., Mignac, D., Nascimento Lima, L., Belyaev, K., and Ji-Ping, X.: The REMO ocean data assimilation system into HYCOM (RODAS\_H): General description and preliminary results, *Atmospheric and Oceanic Science Letters*, 7, 464–470, 2014.
- Tsujino, H., Urakawa, S., Nakano, H., Small, R. J., Kim, W. M., Yeager, S. G., Danabasoglu, G., Suzuki, T., Bamber, J. L., Bentsen, M.,  
620 et al.: JRA-55 based surface dataset for driving ocean–sea-ice models (JRA55-do), *Ocean Modelling*, 130, 79–139, 2018.
- Weaver, A. and Courtier, P.: Correlation modelling on the sphere using a generalized diffusion equation, *Quarterly Journal of the Royal Meteorological Society*, 127, 1815–1846, 2001.
- Weaver, A., Vialard, J., and Anderson, D.: Three- and four-dimensional variational assimilation with a general circulation model of the tropical Pacific Ocean. Part I: Formulation, internal diagnostics, and consistency checks, *Monthly Weather Review*, 131, 1360–1378, 2003.



- 625 Zavala-Garay, J., Wilkin, J., and Arango, H.: Predictability of mesoscale variability in the East Australian Current given strong-constraint data assimilation, *Journal of physical oceanography*, 42, 1402–1420, 2012.
- Zeldis, J. R., Walters, R. A., Greig, M. J., and Image, K.: Circulation over the northeastern New Zealand continental slope, shelf and adjacent Hauraki Gulf, during spring and summer, *Continental Shelf Research*, 24, 543–561, <https://doi.org/10.1016/j.csr.2003.11.007>, 2004.